



Fully Parameterized Finite Element Model of a Grand Piano Soundboard for Sensitivity Analysis of the Dynamic Behavior

Item type	text; Electronic Thesis
Authors	Mokdad, Fatma
Publisher	The University of Arizona.
Rights	Copyright © is held by the author. Digital access to this material is made possible by the University Libraries, University of Arizona. Further transmission, reproduction or presentation (such as public display or performance) of protected items is prohibited except with permission of the author.
Downloaded	17-Nov-2017 15:46:25
Link to item	http://hdl.handle.net/10150/293647

A FULLY PARAMETERIZED FINITE ELEMENT MODEL OF A
GRAND PIANO SOUNDBOARD FOR SENSITIVITY ANALYSIS
OF THE DYNAMIC BEHAVIOR

by

Fatma Mokdad

A Thesis Submitted to the Faculty of the
DEPARTMENT OF AEROSPACE AND MECHANICAL ENGINEERING

In Partial Fulfillment of the Requirements
For the Degree of

MASTER OF SCIENCE
WITH A MAJOR IN MECHANICAL ENGINEERING

In the Graduate College
THE UNIVERSITY OF ARIZONA

2013

STATEMENT BY AUTHOR

This thesis has been submitted in partial fulfillment of requirements for an advanced degree at the University of Arizona and is deposited in the University Library to be made available to borrowers under rules of the Library.

Brief quotations from this thesis are allowable without special permission, provided that accurate acknowledgment of source is made. Requests for permission for extended quotation from or reproduction of this manuscript in whole or in part may be granted by the head of the major department or the Dean of the Graduate College when in his or her judgment the proposed use of the material is in the interests of scholarship. In all other instances, however, permission must be obtained from the author.

SIGNED: _____
Fatma Mokdad

APPROVAL BY THESIS DIRECTOR

This thesis has been approved on the date shown below:

Samy Missoum
Associate Professor of Mechanical Engineering

Date
May 1st, 2013

ACKNOWLEDGEMENTS

I would like to express my sincere gratitude to Dr. Samy Missoum, Chair of my Master thesis committee, for the great learning experience I gained during my Master, through his expertise and enthusiasm for the research topic.

My deepest appreciation goes to my committee members, Dr. Cho Lik Chan and Professor Parviz Nikravesh, for their cooperation, support and interest in my research subject.

Many thanks to the Fulbright Scholarship Headquarters in Washington, DC, and my Amideast advisors Ethan Mapes and Deirdre Evans-Pritchard for their continuous guidance and for providing me with the needed funding to pursue my Master.

I thank all the faculty members of the Aerospace and Mechanical Engineering Department, of the College of Engineering, as well as the Graduate College, for their consideration and clarifications whenever required.

Many thanks to my colleagues, members of the CODES Lab, Christoph Dribusch, Peng Jiang and Sylvain Lacaze for their help and support whenever needed.

Finally, I would like to thank my family members who have always been a great source of motivation and inspiration.

TABLE OF CONTENTS

LIST OF FIGURES	6
LIST OF SYMBOLS	9
LIST OF ABBREVIATIONS	11
GLOSSARY	12
ABSTRACT	14
CHAPTER 1 INTRODUCTION	15
CHAPTER 2 LITERATURE REVIEW	18
2.1 Introduction	18
2.2 Literature Review Summary	18
2.3 Conclusions	24
CHAPTER 3 PRESENTATION OF THE INSTRUMENT	25
3.1 Piano History	25
3.2 Main Components of the Piano	25
3.3 The Piano Soundboard	28
3.3.1 Overall Shape, Geometry and Components	28
3.3.2 Choice of the Wood and Material Properties	30
3.3.3 Soundboard Crownning and Downbearing	32
CHAPTER 4 SOUNDBOARD FINITE ELEMENT MODEL	34
4.1 Introduction	34
4.2 Presentation of the Fully Parameterized Model	34
4.2.1 Geometric Characteristics	34
4.2.2 Choice of the Materials for the Wood	34
4.2.3 Choice of Elements	36
4.3 Crown Implementation	39
4.4 Downbearing Implementation	40
4.5 Parameterization of the Boundaries	46

TABLE OF CONTENTS – *Continued*

CHAPTER 5 MODELING AND ANALYSES TECHNIQUES	48
5.1 Modal Analysis	48
5.2 Prestressed Modal Analysis	49
5.3 Inclusion of Geometric Nonlinearities	49
5.3.1 Harmonic Analysis	51
5.4 Sensitivity Analysis	53
5.4.1 Global Sensitivity Techniques	53
5.4.2 Variance Based Techniques	55
CHAPTER 6 RESULTS	58
6.1 Introduction	58
6.2 Downbearing: Linear and Geometrically Nonlinear Approaches	58
6.3 Competing Effects of Crowning and Downbearing	63
6.4 Influence of the Nature and Type of the Boundary Conditions	66
6.5 Effects of the Soundboard Ribs on the Eigen-modes	68
6.6 Influence of the Variation of the Thickness Distribution	70
6.7 Sensitivity Analysis Results	72
6.7.1 Preliminaries	72
6.7.2 Pearson Linear Correlation Coefficients (PLCC)	72
6.7.3 Spearman Rank Order Correlation Coefficients (SRCC)	73
6.7.4 Results of the Variance Based Techniques: Sobol Indices	73
6.8 Harmonic Analyses Results	78
6.9 Conclusions	79
CHAPTER 7 DISCUSSION AND FUTURE WORK	82
APPENDIX A CHOICE OF THE MESH SIZE	84
APPENDIX B DOWNBARING: COMPARISON BETWEEN THE TWO IMPLEMENTATION TECHNIQUES	86
APPENDIX C MODAL SHAPES AND NODAL SOLUTIONS FOR THE FIRST SEVEN EIGEN-MODES	88
APPENDIX D MODE SHAPES VS. CHLADNI PATTERNS	90
REFERENCES	91

LIST OF FIGURES

1.1	Main Components of a Grand Piano (Blackham, 1965)	17
3.1	Original Cristofori Pianoforte (Schott, 1993)	26
3.2	The Playing Mechanism of a Grand Piano (Overs, 2012)	26
3.3	Grand Piano Strung Back (Overs, 2012)	27
3.4	Case of a Grand Piano: Rim Highlighted (Overs, 2012)	27
3.5	Feathered Ribs of the Soundboard (Chabassier and Chaigne, 2011) .	30
3.6	Top View of the Bass Bridge (Short) and Treble Bridge (Long) (Overs, 2012)	30
3.7	Quarter-sawn Strips of the Wood	31
3.8	Cutting of Spruce Planks: Wood Directions (Ege, 2009)	31
3.9	Positioning of the Strings on the Bridges (Chabassier, 2012)	32
3.10	Simplified Scheme of Crowning then Downbearing of the Soundboard (Mamou-Mani, 2007)	33
4.1	2.74 m Grand Piano Soundboard (Left), Finite Element model (Right) .	35
4.2	Geometric Parameters of the Soundboard: Board and Bridges (Up), Zoom on a Rib (Down)	36
4.3	Element Type Shell43 (Kohnke, 1999)	38
4.4	Element Type Beam188 (Kohnke, 1999)	39
4.5	Element Type Link8 (Kohnke, 1999)	39
4.6	Element Type MPC184 (Kohnke, 1999)	40
4.7	Crowning for Radii of Curvature $R_c = 5, 15$ and 50 m (From Left to Right Respectively)	41
4.8	Individual String Tensions for a 2.74 m Grand Piano (Conklin Jr, 1996a)	42
4.9	Individual Speaking Lengths for a 2.74 m Grand Piano (Conklin Jr, 1996b)	42
4.10	Simplified Model For a Single String	43
4.11	Example of Downbearing Force Distribution	43
4.12	Position of the Strings on the Soundboard	44
4.13	Implementation of the Strings in the Model	44
4.14	Forces on a String ((x,y) is the Plane of the Soundboard)	45
4.15	Inclusion of the Equilibrium Forces in the Model	45
4.16	Front View of the Lateral Width of the Boundary Area (Tippner et al., 2006)	46

LIST OF FIGURES – *Continued*

4.17	Parameterized Boundary Areas for $p_b = H_2/10, H_2/25, H_2/50$ and $H_2/100$ (From Top Left to Bottom Right Respectively)	46
5.1	First Iteration of NR (Kohnke, 1999)	50
5.2	Iterations of NR (Kohnke, 1999)	51
5.3	FRF Plot Showing the Different Parameters Needed to Compute the Quality Factor Q	52
5.4	Scatter Plot Showing a Linear Relationship Between an Input X and an Output Y	54
5.5	Scatter Plot Showing a Nonlinear Monotonic Relationship Between an Input X and an Output Y	54
6.1	Effects of Variation of the Strings Tension on a Flat Soundboard for the 1 st and 2 nd Frequencies: Linear (Dashed), Geometrically Nonlinear (Solid)	60
6.2	Effects of Variation of the Strings Tension with $R_c = 50\text{ m}$ for the 1 st and 2 nd Frequencies: Linear (Dashed), Geometrically Nonlinear (Solid)	61
6.3	Effects of Variation of the Strings Tension with $R_c = 35\text{ m}$ for the 1 st and 2 nd Frequencies: Linear (Dashed), Geometrically Nonlinear (Solid)	62
6.4	Effects of Variation of the Strings Tension with $R_c = 15\text{ m}$ for the 1 st and 2 nd Frequencies: Linear (Dashed), Geometrically Nonlinear (Solid)	63
6.5	Effects of the Crowning Without Accounting for the Strings Tension: First Two Natural Frequencies	64
6.6	Effects of the Crowning when Accounting for the Actual Amount of Strings Tension: First Two Natural Frequencies	65
6.7	Coupled Effects of Crowning and Downbearing on the 1 st Natural Frequency	67
6.8	Feathered Ribs of the SB with $r_2=1/3$ and $1/8$ (From Left to Right Respectively)	69
6.9	Variation of the Feathering Height From $h_f=h_r/10$ (Left) to $h_f = h_r(Right)$	69
6.10	MAC Matrix Resulting From the Alteration of the Height of the Ribs Feather	70
6.11	Thickness Distribution of the Board For a Taper Ratio $r_3 = 1/3$	71
6.12	Influencing Inputs on the 1 st Natural Frequency (by means of Spearman Rank Correlation Coefficients)	74
6.13	Influencing Inputs on the 2 nd Natural Frequency (by means of Spearman Rank Correlation Coefficients)	74

LIST OF FIGURES – *Continued*

6.14 Influencing Inputs on the 3 rd Natural Frequency (by means of Spearman Rank Correlation Coefficients)	75
6.15 Total Effect Sobol Indices for the 1 st Natural Frequency	76
6.16 Total Effect Sobol Indices for the 2 nd Natural Frequency	77
6.17 Total Effect Sobol Indices for the 3 rd Natural Frequency	77
6.18 FRF of the Displacements on the <i>z</i> Direction (DMP ratio $\xi = 0.02$) .	78
6.19 FRF of the Displacements on the <i>Z</i> Direction (DMP ratio $\xi = 0.04$) .	80
A.1 Convergence of the First Five Natural Frequencies with Respect to the Mesh Size	85
A.2 Convergence of the First Five Natural Frequencies with Respect to the Mesh Size: Zoom on the Convergence Zone	85
C.1 Deformed Shapes Relative to the First Seven Eigen-modes: From Mode 1 (Top Left) to Mode 7 (Bottom) Respectively.	88
C.2 Nodal Displacements Relative to the First Seven Eigen-modes	89
D.1 Chladni Patterns (Conklin Jr, 1996a) Vs. FEM Mode Shapes For the First Three Natural Frequencies	90

LIST OF SYMBOLS

Symbol	Description	Units
$[C]$	Damping matrix	Ns/m
DEN_b	Density of the SB	Kg/m^3
DEN_r	Density of ribs and bridges	Kg/m^3
D_w	Amount of downbearing	N
E_{Lb}	Longitudinal Young modulus of the SB	GPa
E_r	Young Modulus of ribs and bridges	GPa
E_{Tb}	Transverse Young modulus of the SB	GPa
f	Frequency along a string	Hz
$\{F_a\}$	Vector of applied loads	N
F_d	Downbearing force	N
F_i^{nr}	Vector of restoring loads	N
h_b	Height of the bridges	m
h_f	Feathered height of the ribs	m
h_r	Main height of the ribs	m
K	Stiffness of the springs	N/m
$[K]$	Stiffness matrix	N/m
$[K_g]$	Geometric stiffness matrix	N/m
$[K_g^*]$	Geometric stiffness due to a unitary load	N/m
$[K_{mat}]$	Material stiffness matrix	N/m
$[K^T]$	Tangent stiffness matrix	N/m
L_r	Total length of a rib	m
$[M]$	Mass matrix	Kg
N_r	Total ribs number	NA
p_b	Parameter for width of the boundary	m
Q	Quality factor	NA
r_1	Feathering taper ratio	NA
r_2	Feathering start ratio	NA
r_3	Thickness tapering ratio	NA
S_i	First order Sobol indices	NA
S_{ci}	Complementary Sobol indices	NA
$S_{i,ci}$	Coupled effects Sobol indices	NA
S_{T_i}	Total effects Sobol indices	NA
r_i	Load residual in NR method	N

LIST OF SYMBOLS - *Continued*

Symbol	Description	Units
R_c	Radius of curvature	m
T	The string tension	N
$\{u\}$	Vector of unknown DOF	m
w_r	Width of the ribs	m
δ_w	Deflections along the bridges	m
μ	The mass per unit length of a string	Kg/m
λ	Max displacement induced by the load	m
ζ	Damping ratio of the structure	%
ω	Angular velocity	rd/s
Δf	Bandwidth	Hz

LIST OF ABBREVIATIONS

APDL	ANSYS Parametric Design Language	16
CRW	Crowning.....	64
DACE	Design and Analysis of Computer Experiments	56
DMP	Damping	66
DOF	Degrees Of Freedom	38
DWB	Downbearing	66
FEM	Finite Element Method	24
FREQ	Frequency	59
FRF	Frequency Response Function.....	52
MAC	Modal Assurance Criterion	69
NA	Not Applicable	9
NR	Newton Raphson	50
PLCC	Pearson Linear Correlation Coefficients	72
SRCC	Spearman Rank order Correlation Coefficients	73

GLOSSARY

Action: Assembly of hammers, dampers and piano keys, that is excited once the key is pressed	26
ANSYS: Commercial software package for analyzing structures using Finite Element Method	16
Boundary Conditions: Constraints imposed on the boundaries of a structure.....	16
Bridge: Wooden strip on the top of the board connecting vibrating strings to the soundboard	15
Damping: Measure of the rate at which the decay of a free vibration happens. Vibrations decay slowly for a high damping system.....	22
Damper: Belongs to the piano action. Its function is to stop the string vibration promptly once the key is released.....	26
Eigen-mode: Mode of vibration characterized by a natural shape and an associated frequency	22
Finite Element Method: Technique of analyzing structures by dividing them into elements.....	16
Fortissimo: Stands for playing musical instruments very loudly	15

GLOSSARY- *Continued*

Hammer: Component in the piano action that has as function to strike the string when a key is played	21
Keyboard: Formed by a number of keys (usually 88) assembled within a keyframe. Each key applies to its specific action and damper assembly.....	26
Orthotropic: Said about materials that, such as wood, have properties that vary in orthogonal directions	20
Pedals: Components placed on the legs of the piano. They affect the piano tone once activated	26
Pianissimo: Stands for playing musical instruments very quietly.....	15
Ribs: Bars attached to the bottom of the soundboard and have as function to stiffen the board	16
Speaking Length: Corresponds to the length from the contact point at the bridge to the keyboard	28
Timbre: Perceived sound quality of a note.....	15
Tone: Character of a sound which constitutes the unique difference between voices of the same instrument	18

ABSTRACT

The main objective of this thesis is to understand the mechanics of a grand piano soundboard and to investigate the influence of several parameters on its modal and vibrational behaviors. Various analysis techniques are made possible by a development of a fully parameterized Finite Element model of the soundboard which allows the user to modify most geometric and material parameters. In addition, two crucial features, namely crowning and downbearing, are included in the model and their individual and combined effects are observed. This study also accounts for the influence of geometric nonlinearities due to downbearing.

The piano soundboard includes a large number of unknown factors stemming from its construction process and the material properties of the wood. This thesis uses sensitivity techniques to investigate the influence of various factors on the variability of the modal outputs (i.e., natural frequencies and mode shapes). The different aspects of the model are described in details and various sensitivity methods are tested in this context.

Keywords: Soundboard, vibrational behavior, Finite Element, crowning, downbearing, geometric nonlinearities, sensitivity analysis, modal outputs, natural frequencies, mode shapes.

CHAPTER 1

INTRODUCTION

The piano has been one of the most distinguished musical instruments in the world for centuries. It has the ability to produce different timbres when a pianist alters the striking force which generates varying volumes. Understanding the mechanics of the grand piano and its sound production represent longstanding goals for anyone interested in the behavior of this sophisticated instrument. Musicians as well as engineers have been intrigued with its overall complexity (Conklin Jr, 1996b).

In general, the piano has 88 keys and 230 strings (Giordano, 1997), and produces notes ranging over 7 octaves from A_0 to C_8 , following a dynamic range of 60 dB from pianissimo to fortissimo (Keane, 2006). Among the over ten thousand components of a grand piano, the soundboard represents one of the most complicated parts. Its purpose is to transform the string vibrations, transferred through the bridges, into sound (Giordano, 1997). That is, the soundboard which has a much larger area than the strings, acts as an “amplifier”. The design of this radiating component is of tremendous importance and will substantially dictate the “quality” of the piano timbre.

There are many design and manufacturing parameters involved in a soundboard and there are still many questions related to their relative influence. Among the factors contributing to the dynamic behavior of the piano soundboard, geometry and material properties of the wood are well known and intuitive parameters. However, other factors such as its initial crowning and the effect of downbearing (i.e., the forces due to the strings tension), are of prime importance and have been shown to influence the dynamic behavior of the piano soundboard significantly.

Both crowning and downbearing result in prestresses in the soundboard. Crown-

ing is a step of the manufacturing process that produces a curvature in the soundboard plate and downbearing refers to the downward forces exerted by the tensioned strings onto the soundboard, via the bridges. The adjustments and interactions of crowning and downbearing are crucial in order to preserve the high quality of the instrument.

Concerning the boundary conditions, the soundboard is assumed to be vibrationally terminated around its ends. However, the type of termination that connects its edges to the case in which it is fitted, appears to be between the simply supported and the totally clamped conditions (Ortiz-Berenguer et al., 2008). The lateral width assumed as boundary has also a big influence on its eigen-frequencies (Keane, 2006). Consequently, to precisely study these various aspects, a Finite Element model of the soundboard was implemented in ANSYS Parametric Design Language (APDL).

In order to study the effects of the most common parameters, this work introduces a fully parameterized Finite Element model of a piano soundboard. The model includes the plate, the feathered ribs running diagonally across its backside, the elevated curved bridges on the top of it (i.e., the bass and the treble bridges), and the strings. This model enables the user to entirely specify the geometry, the dimensions of the bridges and ribs, number and angles of ribs, and other geometric parameters such as rib feathering. In addition, the model implements a user-defined crowning of the soundboard and downbearing due to the strings is also implemented.

The types of boundary conditions and the areas to which they are applied can be easily prescribed. Beside the parametric model, this thesis presents global sensitivity analyses of the responses (i.e., natural frequencies) with respect to the chosen parameters. The role of geometric nonlinearities will be considered in the study of the dynamic behavior of the soundboard, including the investigation of competing effects of crowning and downbearing and the effect of boundary conditions.

This thesis is organized as follows: Chapter 2 presents a comprehensive literature review. Chapter 3 introduces the piano and its various components with a special

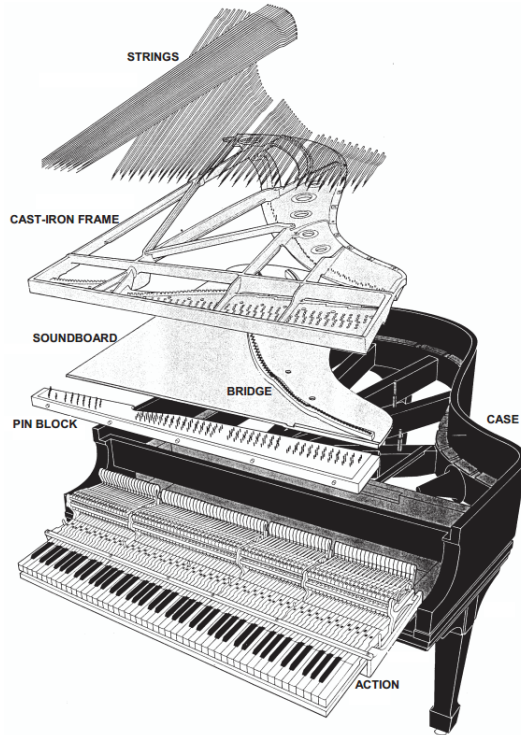


Figure 1.1: Main Components of a Grand Piano (Blackham, 1965)

focus on the soundboard. Chapter 4 describes the construction of the fully parameterized Finite Element model in terms of geometry, material properties, boundary conditions, and prestresses. Chapter 5 is dedicated to the solution techniques to analyze the dynamic behavior of the soundboard and the sensitivity methods to study the influence of various factors. Finally, Chapter 6 presents the most relevant results, followed by a discussion in Chapter 7.

CHAPTER 2

LITERATURE REVIEW

2.1 Introduction

This chapter reviews the research papers and articles that were used to cover various aspects of the soundboard design and analyses. It will be presented under the following sections:

- Modeling of the piano soundboard
- Modal analyses and model validation
- Dynamics and vibrational behavior of the soundboard
- Sound production through the soundboard
- Sensitivity analysis of the most influencing parameters

2.2 Literature Review Summary

Modeling of the Piano Soundboard: Realistic modeling of the piano soundboard represents a complicated task. Many researchers have been interested in finding the most accurate way to achieve the soundboard modeling (e.g., FEM, analytical representation...).

The earliest studies in the area are credited to Bilhuber (Bilhuber and Johnson, 1940). Through his modeling, he was interested in the soundboard and its affect on the acoustical quality of the piano. Using his experimental results, he has proven that the vibrational behavior of the soundboard is directly dependent on the strings loading. He showed that the quality of the piano tone is highly improved when the responsiveness of the soundboard is changed. Therefore, he proposed to alter

various characteristics of the board (e.g., tapering the thickness on the edges to reduce its mass, raising the plane of the treble bridge...). As a result, he has proven that he could increase the duration of the tone (i.e., what he called “liveliness” of the piano).

The studies conducted by Mamou-Mani (Mamou-Mani et al., 2008) consisted of building a Finite Element model using CAST3M software in order to determine the effect of downbearing on the soundboard vibrations. This study included the presence of ribs, bridges as well as the board crowning. The work was performed using two methods to account for prestresses (i.e., a linearized approach and a geometrically nonlinear approach). A 1.8 m IBACH piano soundboard was considered for the studies. In a more detailed publication (Mamou-Mani, 2007), he explained that downbearing was applied via a vertical force per unit length on the bridges and modeled with a geometric nonlinear approach with prestress. He has shown that for an initially flat soundboard, the eigen-frequencies increased with downbearing. However, for a board with an initial crown, downbearing effects are in opposition to the crowning. Frequencies of the first seven modes of the soundboard were also studied for clamped, fixed, and free boundary conditions.

The purpose behind Kean’s research (Keane, 2006) was to improve the upright piano through modifications of the material properties of the soundboard. In his case, both upright and grand piano soundboards were modeled using Finite Element Analysis and modal frequencies were found. He has shown that it is particularly challenging to find out how to produce the best sound in a piano. He went into more depth in the study of upright piano soundboards and their sound production. He also provided useful insight into soundboard modeling that included effects from the rim and the sound radiation due to the case. His consideration of loosely clamped versus fully clamped boundary conditions gave rise to the way piano boundaries should be accurately modeled.

Chabassier (Chabassier, 2012) paid more interest to the numerical simulations of

the piano using physical models. Her model discretization was based on numerical approximations in space. Her objectives were to come out with a scheme allowing to preserve the energy for a nonlinear system of equations. She goes into details of vibroacoustics concerning the spatial discretization and the temporal scheme (Chabassier and Chaigne, 2011).

Modal Analyses and Model Validation: Once the type of modeling is chosen, the next step is to define the nature of the output that would be interesting to observe in order to predict the behavior of the structure.

A study performed by Berthaut (Berthaut et al., 2003) focused on predicting the behavior of the piano soundboard using Finite Element models as well as analytical models. He validated his modeling through experimental modal analysis using a 2-D finite element of a Pleyel P190 soundboard. The model was generated with close attention to the influence of the ribs, orthotropic material properties of the board, and clamped boundary conditions. Validation with the analytical model was completed through the use of Modal Assurance Criterion (MAC). Berthaut concluded that numerical modeling produced good results at a high cost whereas analytical modeling was much simpler but produced lower precision. Overall, his study claimed that the Finite Element Method is very accurate in describing the dynamical behavior of a piano soundboard.

Ortiz-Berenguer (Ortiz-Berenguer et al., 2008) examined the vibrational characteristics of the soundboard based on the affects of the ribs. Both the real and imaginary parts of the mechanical impedance of a Yamaha C7 soundboard were measured experimentally. In addition, in this study, a Finite Element model of a soundboard was modeled using ANSYS software. In order to validate his model, experimental frequencies were tested on the C7 soundboard and compared to frequencies evaluated in ANSYS. Six different simulated plates were modeled: From a simple rectangular isotropic plate up to a piano-shaped orthotropic plate with

accurate material properties and with ribs and bridges included. He found that the most detailed plate produced the most accurate modal results and provided a good estimate for the impedance of the piano soundboard.

Dynamics and Vibrational Behavior of the Soundboard: The purpose from the modeling of the soundboard is to obtain a structure that would provide the ability to predict the dynamical and vibrational behaviors realistically.

Through his successive publications, Conklin tried to narrow down the relations between the design of a piano and the quality of its tone through investigations on its vibrational behavior. His focus was based on an instrument designer point of view, which made his publications rather technical. In the first place, he was interested in the hammers and their tonal effects (Conklin et al., 1996). The purpose was to determine a certain relation between the shape and design of the piano and the quality of its tone. The second part of his publication series (Conklin Jr, 1996b) was the most relevant to our research since the focus was brought to the soundboards. Various aspects were taken into account such as the material properties of the different components of the soundboard as well as its geometry and its interaction with the rest of the piano components. This publication will be brought up in various occasions through this thesis. The last part of the series (Conklin Jr, 1996a) is about the piano strings, their types and their longitudinal modes. Several aspects of the strings were considered such as the inharmonicity and the wrapping.

Giordano (Giordano, 1997) studied the mechanical impedance of the soundboard. He considered the effects of string stiffness, connection of string to the soundboard, nonlinear behavior of the hammers, and the complicated geometry of the soundboard as relevant problems in the modeling. For his investigations, a simple Finite Element model of a square board was generated in order to find the vibrational properties. He varied the material properties from isotropic to anisotropic while considering the influence of the ribs. A study of the impedance of each of these configurations

was carried out. His model did not resemble a piano soundboard geometrically. However, his study represents one of many steps in determining how to calculate the sound produced in a piano.

Later, Giordano (Jiang and Giordano, 2004) reported a study in which he conducted an experimental study of the impedance of a piano soundboard. He presented which aspects of the piano contribute to its performance and sound. He evaluated his results by comparing them to Wogram (Wogram, 1990) and found great differences between the two. That is, in contrast to the findings of Wogram, Giordano confirmed that the ribs have a dominant effect on the natural frequencies, through various experiments using driving points along an upright piano bridge.

Suzuki (Suzuki, 1986) reported on a modal analysis and surface-intensity methods to determine vibration and radiation characteristics of a piano soundboard. He examined the differences in sound radiation at various frequency ranges. Moreover, he used a curve fitting algorithm in order to calculate the frequency and damping of a Steinway model L soundboard. Mode shapes were found and the intensity patterns for the board were determined based on three different driving points along the bridge. He mentioned that the accuracy of the surface-intensity method had major drawbacks due to the calibration of the equipment, but he found that the intensity patterns change in complex ways as the frequency is varied.

Moore and Zietlow explored the deformation shapes of an upright piano soundboard via electronic speckle pattern interferometry (Moore and Zietlow, 2006). Their results were compared against those obtained from a Finite Element model. The Finite Element model had assumed isotropic material properties. Moore and Zietlow were able to determine that the pressure of the strings on the soundboard generates significant changes in the mode shapes and resonant frequencies. Their findings are particularly useful when considering which properties of the soundboard must be included in the model in order to generate an accurate representation.

Sound Production Through the Soundboard: The main objective from the representation of the soundboard is to learn the details about its vibrational characteristics. The soundboard is the amplifier of the piano which has a direct relation with the sound production and the quality of the piano tone.

Giordano and Jiang (Jiang and Giordano, 2004) studied the physical modeling of the piano with a focus on the interaction between hammer and string. Mechanical impedance was used to judge the behavior of the board and compared experimentally to an actual one. Models were done considering the ribs and the bridges as well as the material properties of the board. Although little attention was given to the characteristics of the soundboard, this study is important since it considers potential coupling effects from other components, such as the coupling between the hammer and the strings. They elaborate further on the mechanics of the soundboard, explaining the interaction between the vibrating strings, the bridges, and the board.

Fletcher and Rossing (Fletcher and Rossing, 1998) identified several aspects of the soundboard, related to the sound production. Mode shapes were presented to help describe the sound radiation and the soundboard impedance. In addition, decay rates were shown to demonstrate the interactions between strings, bridges, and soundboard. Their main concern was on the coupling of the strings to the bridge and the sound decay of the piano.

Sensitivity Analysis of the Most Influencing Parameters: Various characteristics are involved within the piano soundboard. In order to depict the most influencing factors, sensitivity analysis is of a great use since it allows to classify the outputs based on their influence on the behavior of the structure.

Tippner (Tippner et al., 2006) studied the influence of various factors on the dynamical behavior of a piano soundboard by looking at the natural frequencies and the mode shapes based on a Finite Element model. The considered soundboard

was a Petrof-IV having orthotropic material properties. Sensitivity analysis was performed on the declination angle of the grain of the wood, the wood density and the thickness of the board. Their effects on the natural frequencies were observed. In addition, various configurations were tested and modal characteristics have been shown to be highly influenced by material properties.

2.3 Conclusions

Most researchers validated their models experimentally. Others provided empirical models simulating actual soundboards. Few models mentioned dynamical aspects such as the influence of the board crowning or the downbearing effects brought by the strings, which will be of high interest in this thesis.

The purpose of the preceding literature review was to introduce the various topics that were targeted along our research. Many of the discussed studies were interesting since they included the modeling of the soundboard using FEM, which allowed us to develop a fully parameterized model that can accommodate any piano shape and any user defined parameters and to be able to use it for the study of vibrational behavior of the soundboard.

CHAPTER 3

PRESENTATION OF THE INSTRUMENT

3.1 Piano History

The popularity of the piano has been increasing since the 18th century for being one of the most appreciated instruments used in classical or contemporary music. It was first known as a pianoforte when invented by Bartolomeo Cristofori back in 1720. His idea was to develop an instrument that would be able to produce both quiet (piano) and loud (forte) sounds, which gave rise to the name pianoforte. This was contrasting to the harpsichord, which, by having plucked strings, is unable to express various degrees of loudness. Originally, pianoforte was smaller than the grand piano of today and its tonal range was only 5 octaves (Figure 3.1). It had a square shape with a straight bridge.

Following the initial invention, John Broadwood (1777) started making improvements on the piano and changed its shape from the square to the current one. In 1788, he came up with the idea of dividing the bridge which brought improvements to the bass tones. He also had increased the piano range to six octaves by 1794, then to seven octaves by 1820 (Rumsey and Hanggi, 2008). Therefore, the piano had gained more popularity and masterful composers such as Ludwig van Beethoven and Wolfgang Amadeus Mozart realized its expressive nature and wrote music specifically for it (Giordano and Hansen, 2011).

3.2 Main Components of the Piano

Main components of the piano can be enumerated as follows:



Figure 3.1: Original Cristofori Pianoforte (Schott, 1993)

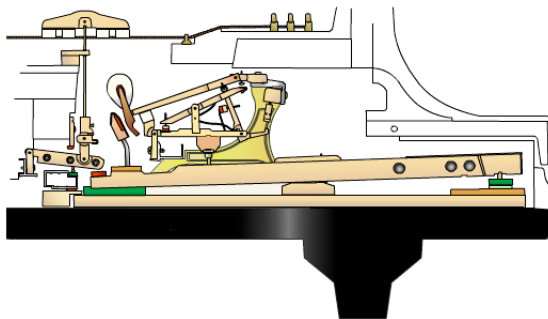


Figure 3.2: The Playing Mechanism of a Grand Piano (Overs, 2012)

- **The Playing Mechanism:** It represents the most complicated chain in the piano. It involves various components that need to work together to provide the piano sound (Figure 3.2). It is composed of the action, the damper, the pedals and the keyboard. Together, they assure the transmission of the energy to the strings.
- **The Strung Back:** It is composed of the top frame, the soundboard and the back frame (Figure 3.3). This component has the function to produce and amplify

the sound of the piano.

- **The Case:** It is mainly composed of the rim (formed of three different parts: the spine, the bentside and the tail) and the lid (Figure 3.4). It represents the total wooden housing of the piano.



Figure 3.3: Grand Piano Strung Back (Overs, 2012)



Figure 3.4: Case of a Grand Piano: Rim Highlighted (Overs, 2012)

3.3 The Piano Soundboard

The overall shape, geometry and components of the soundboard will be described, as well as its material properties and its most relevant features.

3.3.1 Overall Shape, Geometry and Components

The shape of the soundboard results from the number and the length of the strings required to produce the correct sound frequencies. With each string comes a vertical pressure on the bridges. Primarily, this tension is supported by the cast iron frame situated on top of the soundboard (Stulov, 2005). When the strings vibrate, they cause the bridge to vibrate as well, which generates a mechanical energy transformed into acoustical energy through the soundboard. Because the soundboard is very thin, typically the thickness ranges from 6 mm around its edges to 15 mm at the center (Conklin Jr, 1996b), the mechanical energy from the strings easily excites the board (Fletcher and Rossing, 1998).

Main components of the soundboard can be enumerated:

- **The Ribs:** The ribs, also called stiffeners or belly bars, are made to strengthen the structure of the soundboard. They are attached to its bottom opposing the bridges and have the function to stiffen the individual planks of the board (Jiang and Giordano, 2004). The ends of the ribs are feathered to facilitate the rim fitting (Figure 3.5).
- **The Bridges:** The bass and the treble bridges assure the contact and the coupling between the strings and the board. Their main function is to transfer horizontal and vertical vibrations of the strings to the soundboard (Fletcher and Rossing, 1998). The two bridges are assigned such that one is for the bass strings and the other is for the treble strings (Figure 3.6). Position and shape of the bridges are defined based on the number and the speaking lengths of the strings required to produce the full range of sound for the total keys. In addition, the

curved nature of the bridges accommodate both bass and treble strings without having to increase the width of the board.

- The Strings: Although the strings are attached to the cast iron plate that is placed on the top of the board, they have been accounted for as one of the components of the soundboard due to the major impact they have on the bridges. Various features imply the lengths of the strings, so that they can fit accurately on the soundboard (mainly the diameter, the material properties and the required tension). For instance, the bass strings are wrapped with copper material in order to increase the mass per unit length, with a very little increase in stiffness (Conklin Jr, 1996b). Moreover, across the strings, the tension and mass per unit length are varied in order to obtain the proper frequency. This relationship is presented in Eqn.(3.1) which is driven by the string's tension T , its length L and the mass per unit length μ :

$$f = \frac{1}{2L} \sqrt{\frac{T}{\mu}} \quad (3.1)$$

The assumption of an ideal string (i.e., thin, flexible and vibrating transversely) does not imply in reality to the piano strings (Young, 1992). An ideal string is assumed to have vibration modes for which the frequencies form a harmonic series. However, the actual string is characterized by what is called “inharmonicity” (Conklin Jr, 1996b). In fact inharmonicity, meaning the departure from the harmonic series, and which measures the failure of the simple string theory (Schuck and Young, 1973), is inherent to the piano. It is considered as a “defining characteristic” of the tone and a piano without the inharmonicity of the partials would sound unnatural (Conklin Jr, 1996b).

Based on the findings of Young (Young, 1992), inharmonicity of the piano strings can be attributed to their finite bending stiffness. The latest causes a “restoring force”, which adds to the force due to tension. This would have an impact on the modes since it leads to higher frequencies than the true harmonics (Conklin Jr, 1996b).



Figure 3.5: Feathered Ribs of the Soundboard (Chabassier and Chaigne, 2011)

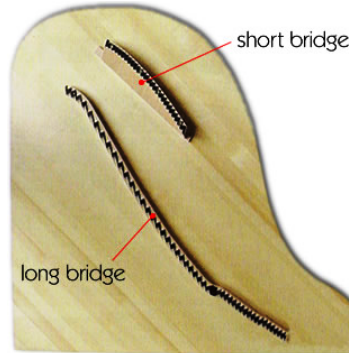


Figure 3.6: Top View of the Bass Bridge (Short) and Treble Bridge (Long) (Overs, 2012)

3.3.2 Choice of the Wood and Material Properties

Piano soundboards are made of solid softwood such as Sitka spruce, which is widely used by manufacturers (Conklin Jr, 1996a). The board is assembled from quarter-sawns, when cutting the lumbers from the original wood log. That is, the log is cut lengthwise into quarters, as presented in Figures 3.7¹ and 3.8.

Sitka spruce is an orthotropic material. It has distinctive and independent material properties in the longitudinal, radial, and transverse directions (Figure 3.8). Table 3.1 displays the different properties that should be considered for an orthotropic

¹ Figure 3.7 was taken from www.wisegeek.org.

material such as the wood of the board.

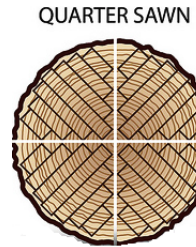


Figure 3.7: Quarter-sawn Strips of the Wood

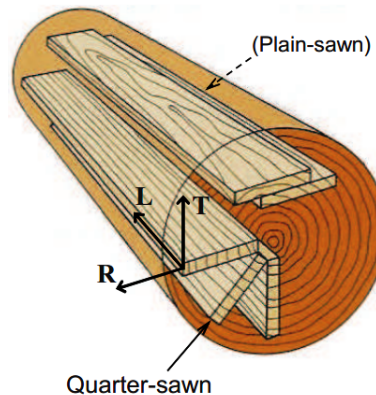


Figure 3.8: Cutting of Spruce Planks: Wood Directions (Ege, 2009)

Table 3.1: Orthotropic Material Properties of the Board

Material Property	Description
$E_{T,L,R}$	Young's modulus: Longitudinal, transverse, radial directions
$G_{TL,LR,RT}$	Shear modulus: T-L, L-R, L-T planes
$\nu_{TL,LR,RT}$	Poisson's ratio: T-L, L-R, L-T planes
ρ	Mass density
ξ	Structural damping ratio

3.3.3 Soundboard Crowning and Downbearing

The soundboard supports a vertical load due to the forces created by the strings (Conklin Jr, 1996a). The forces are transmitted through the bridges (i.e., the bass and treble bridges) (Figure 3.9). To avoid any modeling complexities, most numerical models in the literature (Ege et al., 2012; Mamou-Mani, 2007) have accounted for downbearing roughly as a uniformly distributed force along the two bridges. However, this would imply different amounts of downward forces than what is actually used in piano making, since the speaking length and the tension vary from a string to another (Mamou-Mani et al., 2008).



Figure 3.9: Positioning of the Strings on the Bridges (Chabassier, 2012)

The crown is the curved raised area at the center of the board. Its level is typically measured by its radius of curvature which is usually of the order of 15 to 50 m (Conklin Jr, 1996a). The purpose of the crown is to resist the forces due to the strings (i.e., downbearing) as simplified in Figure 3.10. From a practical point of view, the crown is obtained by gluing the slightly curved ribs across the back of the board and the rim at the periphery. Temperature and moisture content in the wood may also contribute to the formation of the crown (Tippner, 2007).

The crown introduces an elevation in the center of the board by approximately 1 to 2 millimeters (Kindel et al., 1987) which flattens slightly once the strings are applied to the soundboard. When looking at a soundboard, the crown is most likely undetectable, but it has an important role in the overall behavior of the structure. In fact, pianos that have lost their crown due to age or climate, tend to have a duller tone (Giordano and Hansen, 2011).

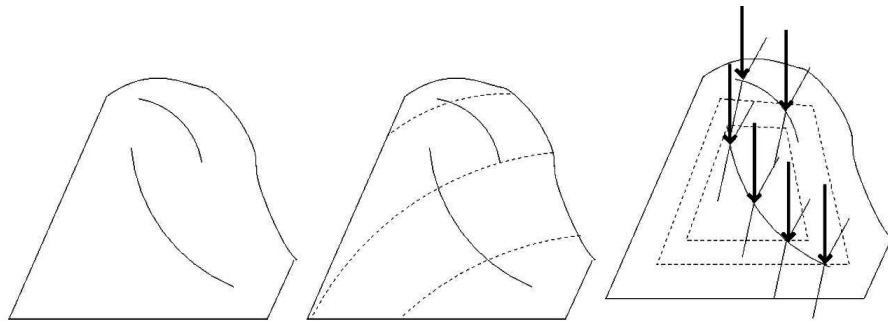


Figure 3.10: Simplified Scheme of Crowning then Downbearing of the Soundboard (Mamou-Mani, 2007)

CHAPTER 4

SOUNDBOARD FINITE ELEMENT MODEL

4.1 Introduction

A numerical model helps forge a better understanding of the soundboard behavior. It introduces an easy way to simulate various configurations and to test them beforehand. A detailed model of a piano soundboard has the ability to provide an insight into its mechanics and its dynamic behavior.

4.2 Presentation of the Fully Parameterized Model

This chapter presents a fully parameterized Finite Element model. The model is automatically built based on a set of user-input parameters. It provides a realistic structure of the soundboard (Figure 4.1)¹.

4.2.1 Geometric Characteristics

The first step in the modeling process is to consider the overall geometry of the soundboard. The design offers a strong simplicity for the user and can be applied to various soundboard geometries. It offers the option to accommodate any shape, once altered. Geometrical parameters are shown in Table 4.1 and Figure 4.2.

4.2.2 Choice of the Materials for the Wood

In the default model, the board is made of Sitka Spruce (Kopač and Šali, 2003) which is orthotropic. Material properties are given in Table 4.2 (Ortiz-Berenguer

¹Actual soundboard in Figure 4.1 was taken from www.piano.christophersmit.com.

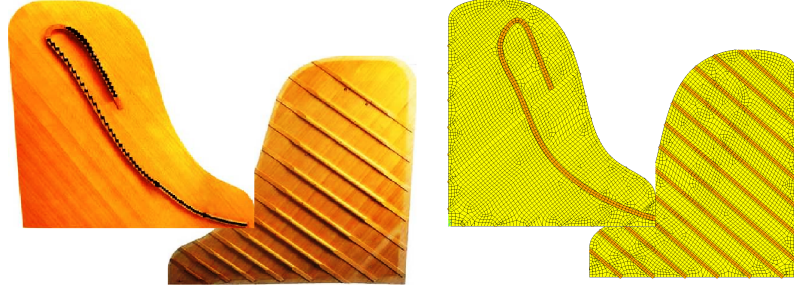


Figure 4.1: 2.74 m Grand Piano Soundboard (Left), Finite Element model (Right)

Table 4.1: Full Soundboard Geometric Parameters

Component	Parameters
The Board	Overall Shape: $H_{1..4}, L_{1..4}$ Main Thickness t_1 Edge Thickness t_2 Wood Grain Angle α_w Thickness Taper Ratio $r_3 = \frac{t_2}{t_1}$
The Ribs	Main Height h_r Feather Height h_f Width w_r Feathering Taper Ratio $r_1 = \frac{h_f}{h_r}$ Total Length L_r Feathered Length L_f Feathering Start Ratio $r_2 = \frac{L_f}{L_r}$ Total Number N_r
The Bridge	Height h_b Width w_b

et al., 2008), where we remind that E represents the Young Modulus, G is the Shear Modulus, ν is Poisson's ratio and ρ is the mass density. Properties are given along the transverse, longitudinal and radial directions of the wood. For the ribs

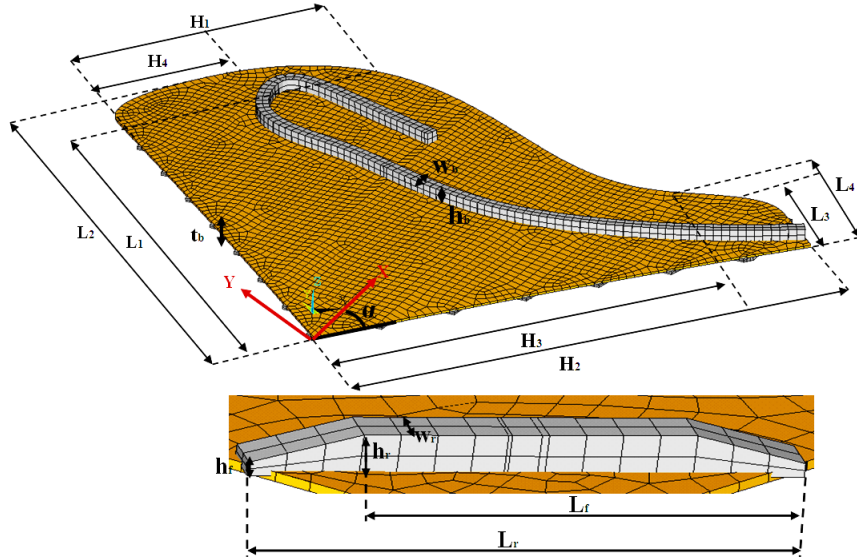


Figure 4.2: Geometric Parameters of the Soundboard: Board and Bridges (Up), Zoom on a Rib (Down)

and bridges, which are made of hard wood (Kopač and Šali, 2003), an isotropic material is used. Note that it is well known that the wood properties can have a wide variability and can be easily altered by the user within the model.

4.2.3 Choice of Elements

The use of FEM takes into account the soundboard area and divides it into many smaller parts referred to as elements. They are connected at their boundaries by a finite number of nodal points. Dividing the soundboard into individual elements, reduces the problem to a finite number of unknowns and a solution is easily approximated. Therefore, meshing (i.e., creating the elements) is among the most crucial steps in developing the soundboard model. It allows for applying the correct materials to the proper component on the soundboard. To accurately mesh the model, the following steps need to be followed:

- Define the attributes for each element type

Table 4.2: Material Properties of the Soundboard Components (Ortiz-Berenguer et al., 2008)

	Board	Ribs and Bridges	
$E_T(GPa)$	0.469		
$E_L(GPa)$	10.9	$E(GPa)$	12
$E_R(GPa)$	0.85		
$G_{TL}(GPa)$	0.665		
$G_{LR}(GPa)$	0.698		
$G_{TR}(GPa)$	0.033		
ν_{TL}	0.025		
ν_{LR}	0.372	ν	0.4
ν_{TR}	0.245		
$\rho(Kg/m^3)$	450	$\rho(Kg/m^3)$	500

- Choose the accurate mesh density
- Generate the mesh

To model the soundboard assembly, four types of elements are considered: A plate to represent the board, beams to represent the ribs and the bridges, links to represent the strings, and rigid beams to simulate the height of the bridges. Table 4.3 represents the element types that were used for each component. Each element admits a set of real constants or section types which define the properties of the material. These different types are summarized below:

Table 4.3: Element Types in ANSYS

Component	Element Type
The board	Shell43
The ribs	Beam188
The bridge	Beam188
The strings	Link8
The rigid beams	MPC184

Element Type: Shell43

To model the main board, shell43 element is used (Kohnke, 1999). It is defined using four nodes I, J, K, and L as shown in Figure 4.3, four thicknesses at each node, as well as orthotropic material properties. This type was selected since it accommodates warped and moderately thick shell structures with variable thickness. This element has the capabilities to give variable thickness throughout the entire board. The first four real constants are assigned to describe the thicknesses at each of the four nodes. The rest of the real constants are not needed and omitted from this model (i.e., element x-rotation and Allman rotation control constants).

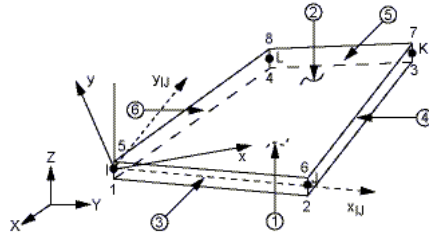


Figure 4.3: Element Type Shell43 (Kohnke, 1999)

Element Type: Beam188

Ribs and bridges are modeled using beam188 (Kohnke, 1999), a three-dimensional finite strain beam, which is defined by two nodes I and J. Figure 4.4 shows the beam orientation in its global coordinate system. It is identified by associating cross sections that may be linearly tapered. This characteristic was particularly useful when modeling the feathered ribs at the edges of the board.

Element Type: Link8

Bass and treble strings are modeled using link8 (Kohnke, 1999), a three-dimensional spar element. It is a uniaxial tension-compression element having three degrees of freedom at each of the nodes I and J (Figure 4.5). This element is defined by its cross-

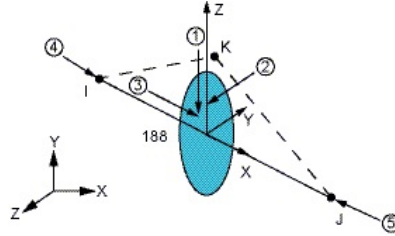


Figure 4.4: Element Type Beam188 (Kohnke, 1999)

sectional area, material properties and initial strain. The characteristic allowing to attribute initial strain to the element would be of great use, when implementing the downbearing effects in the upcoming sections.

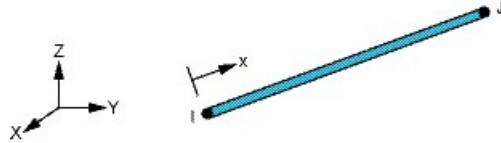


Figure 4.5: Element Type Link8 (Kohnke, 1999)

Element Type: MPC184

The actual height of the bridge was simulated using rigid beam elements MPC184 (Figure 4.6). This element can be used to model rigid constraints between two deformable bodies and it is well suited for linear, large rotation and large strain nonlinear applications. For our application, the strings were attached to the top nodes whereas the bottom nodes were attached to the bridges.

4.3 Crown Implementation

To model the crowning, the soundboard was assigned the shape of a spherical shell (Ege et al., 2012) as presented in Figure 4.7². The curvature is controlled by a

² Note that $R_c = 5$ m in Figure 4.7 is Only Used for Representation Purposes

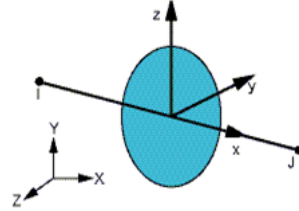


Figure 4.6: Element Type MPC184 (Kohnke, 1999)

user-defined radius of curvature. Practically, depending on the manufacturer, the crown is implemented using one of the following four techniques (Clark, 1998):

Method 1: Known also as the “natural crown”, consists of gluing straight ribs to the board that initially was dried on a flat plateau. Therefore, getting back to the ambient humidity conditions, produces the crown.

Method 2: Consists of gluing curved ribs to the board placed in an initially flat plateau.

Method 3: Consists of gluing straight ribs to the board placed on an initially curved plateau.

Method 4: Consists of gluing curved ribs to the board placed on an initially curved plateau (i.e., ribs and plateau having same amount of curvature). We note that in that case, no prestress effects due to crowning are involved.

4.4 Downbearing Implementation

Two methods are proposed for estimation of downbearing. The main difficulty is that the amount of downbearing changes as function of the deformation of the soundboard.

Method 1: First Iteration Technique

In order to derive the downbearing force, tensions due to each string are first needed. This is made possible using the simple relation between tension and

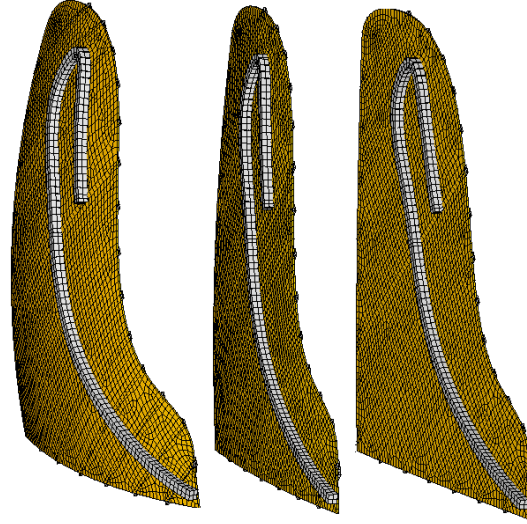


Figure 4.7: Crowning for Radii of Curvature $R_c = 5, 15$ and 50 m (From Left to Right Respectively)

frequency:

$$T_n = 4\mu_n L_n^2 f_n^2 \quad (4.1)$$

where f_n represents the fundamental frequency of a string at the n_{th} key and can be determined, for equal temperament, knowing the standard frequency of the piano (i.e., $f_{A49} = 440$ Hz). T_n is the tension and μ_n is the mass per unit length. The frequencies are given by (Conklin Jr, 1996b):

$$f_n = f_{A49}(2^{\frac{1}{12}})^{(n-49)} \quad (4.2)$$

Tensions and speaking lengths are depicted for individual strings (Figure 4.8 and 4.9), along each key for a 2.74 m grand piano (Conklin Jr, 1996a). Therefore, the mass per unit length for each string can be determined using Eqn.(4.1), where the index n is noted to recall that each string is considered separately (Conklin Jr, 1996b).

From basic statics, one can derive an approximation of the vertical force for a given string (Figure 4.10). When computing the forces and neglecting the deflection,

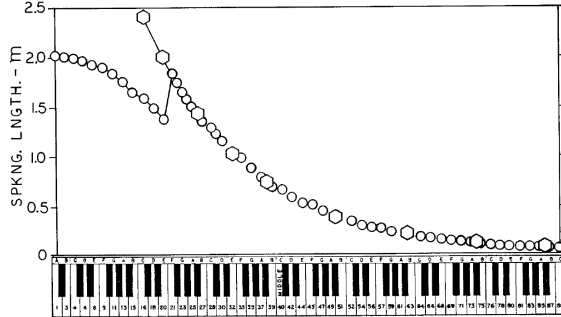


Figure 4.8: Individual String Tensions for a 2.74 m Grand Piano (Conklin Jr, 1996a)

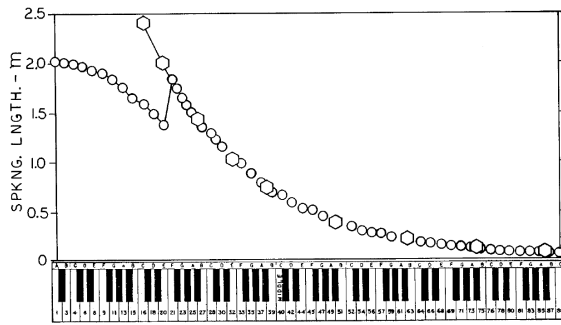


Figure 4.9: Individual Speaking Lengths for a 2.74 m Grand Piano (Conklin Jr, 1996b)

the maximal components will be obtained as:

$$F_n = T_n \sin(\alpha_0) = T_n \frac{h_b}{L_n} \quad (4.3)$$

where α and α_0 are the angles before and after deformation of the soundboard respectively.

Forces are then divided by the maximal force among all the F_n , leading to a unit force for the maximum one. A linear (i.e., small displacement) analysis can then be performed providing the deflections δ_w along the bridges for this loading. The actual vertical displacements, assuming linear behavior, are therefore given by multiplying δ_w by the individual string forces. This provides a first-order

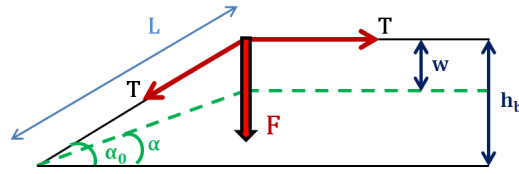


Figure 4.10: Simplified Model For a Single String

approximation of the deflection due to the strings. The amount of downward force can then be updated as follows:

$$F_{dn} = T_n \sin(\alpha_n) = T_n \frac{h_b - w_n}{L_n} = T_n \frac{h_b - F_{dn}(\delta_w)_n}{L_n} \quad (4.4)$$

where a_n denotes the inverse of the speaking length, $a_n = \frac{1}{L_n}$.

The method was implemented in the Finite Element model and the effects of the forces were evaluated with a geometric nonlinear approach (Figure 4.11).

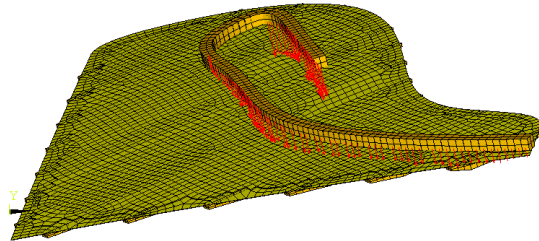


Figure 4.11: Example of Downbearing Force Distribution

Method 2: Actual Representation of the Strings

A second method for approximation of the downbearing forces consists of accounting for the presence of the strings in the model. As pointed before, the strings are attached to the cast iron frame that is superposed to the soundboard (Figure 4.12)³.

³ Before modification, the images in 4.12 were taken from www.piano.christophersmit.com.

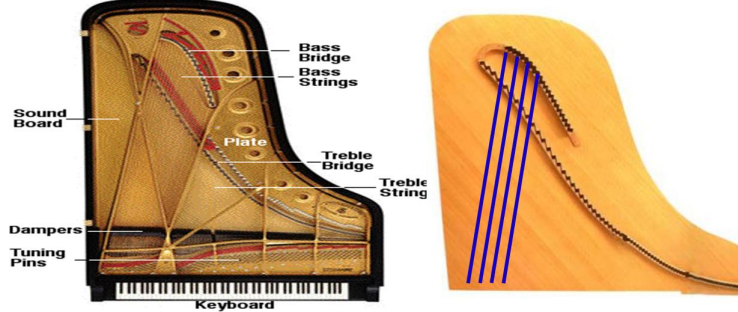


Figure 4.12: Position of the Strings on the Soundboard

We recall that the strings were implemented in the model using the Link8 element type (Figure 4.13), which allows to attribute the initial strain to the element. Knowing the tension relative to each string from Eqn.(4.1), the initial strain is accounted for such as:

$$\varepsilon_n = \frac{T_n}{A_s E_s} \quad (4.5)$$

where A_s represents the cross-sectional area and E_s is the Young's Modulus (usually corresponds to the tempered high-carbon spring steel and admits a value of 210 GPa (Schuck and Young, 1973)).

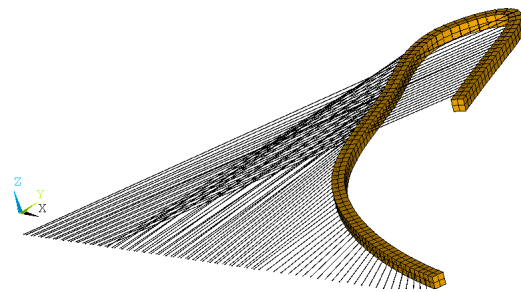


Figure 4.13: Implementation of the Strings in the Model

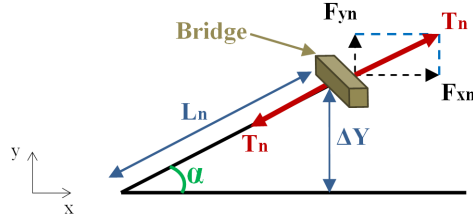


Figure 4.14: Forces on a String ((x,y) is the Plane of the Soundboard)

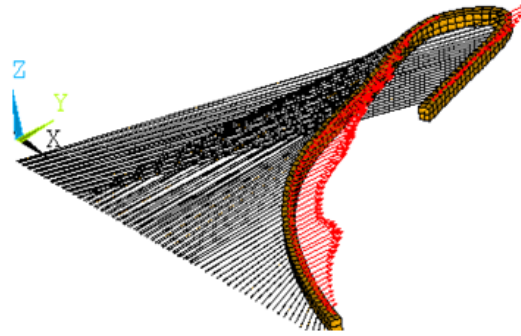


Figure 4.15: Inclusion of the Equilibrium Forces in the Model

In order to satisfy equilibrium, forces acting on the other side of the bridge are also implemented. The forces F_{xn} and F_{yn} for the n_{th} string can be determined based on the angle α_n in the plane (x,y) of the soundboard (Figures 4.14). The implementation in the Finite Element model can be observed in Figure 4.15.

$$F_{xn} = T_n \cos(\alpha_n) \quad (4.6)$$

$$F_{yn} = T_n \sin(\alpha_n) \quad (4.7)$$

The proposed implementation allows us to include stress stiffening effects and downward forces at the contact points of the strings and the bridges. In addition, because the deformation of the board due to downbearing can be rather large compared to the thickness of the board, geometric nonlinearities must be included in the simulation.

A comparison of the two methods, between the natural frequencies for the first five eigen-modes, will be made in Appendix B. All the parameters of the model will be held fixed while varying the downbearing implementation technique for different levels of crown.

4.5 Parameterization of the Boundaries

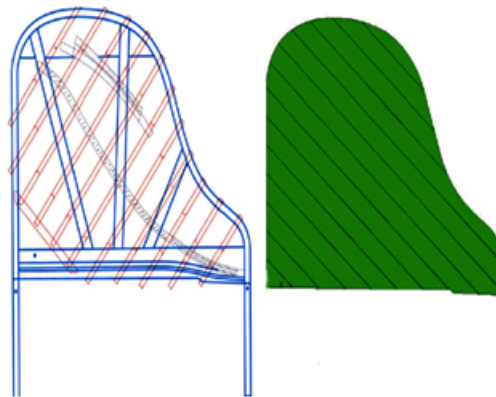


Figure 4.16: Front View of the Lateral Width of the Boundary Area (Tippner et al., 2006)

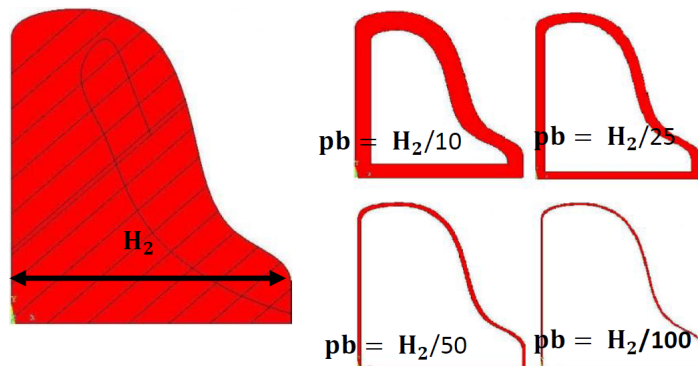


Figure 4.17: Parameterized Boundary Areas for $p_b = H_2/10$, $H_2/25$, $H_2/50$ and $H_2/100$ (From Top Left to Bottom Right Respectively)

Boundary conditions are not obvious and are noted in the literature to be somewhere between the clamped and the simply supported (Berthaut et al., 2003). In addition, the lateral width that is assumed as boundary (Figure 4.16) may vary from one model to another depending on how the piano is assembled and which technique is used by the manufacturer. As a result, the lateral boundary area is parameterized in the model. The user needs only to introduce the parameter p_b function of the main width of the board⁴ H_2 and the boundary area will be automatically generated (Figure 4.17).

⁴Refer to the soundboard scale in Figure 4.2.

CHAPTER 5

MODELING AND ANALYSES TECHNIQUES

5.1 Modal Analysis

Modal analysis is of tremendous importance since it allows to determine the eigen-modes (i.e., natural frequencies and mode shapes). In the simplest case, while disregarding the damping, the discretized equations of motion through Finite Element formulation can be written as:

$$[K] \{q\} + [M] \{\ddot{q}\} = \{g(t)\} \quad (5.1)$$

where $[M]$ is the mass matrix, $[K]$ is the stiffness matrix, q represents the generalized coordinates and g is the load vector. The respective eigenvalue problem has the form:

$$[K] \{q\} = \{\omega^2\} [M] \{q\} \quad (5.2)$$

where $\{\omega\}$ represent the angular velocities and are simply related to the eigen-frequencies by $\{\omega\} = 2\pi \{f\}$. The equation Eqn.5.3 is the key to determining the natural frequencies:

$$|([K] - \{\omega^2\} [M])| = 0 \quad (5.3)$$

The eigen-modes (i.e. the eigen-vectors of $([K] - \{\omega^2\} [M])$) may then be solved for.

From the point of view of model solution, defining a modal analysis requires specifying the number of modes that need to be extracted and the frequency range the user is interested in. Also the mode extraction method (e.g., block lanczos, subspace iteration, damped system using QR algorithm...), as well as the equation solver (e.g.,

front, sparse, jacobi conjugate gradient, incomplete cholesky conjugate...) can be chosen (Kohnke, 1999).

5.2 Prestressed Modal Analysis

In the linear case (i.e., assuming the static displacements are small), the prestressed equations of motion can be written as (Mamou-Mani et al., 2008):

$$([K_{mat}] + [K_g]) \{q\} + [M] \{\ddot{q}\} = \{g(t)\} \quad (5.4)$$

where $[M]$ is the mass matrix, $[K_{mat}]$ is the material stiffness matrix, $[K_g]$ is the geometric stiffness matrix due to prestresses, q are the generalized coordinates and g is the load vector. The eigen-modes in that case can be obtained by solving the following equation:

$$\left| ((([K_{mat}] + [K_g]) - \{\omega^2\} [M])) \right| = 0 \quad (5.5)$$

5.3 Inclusion of Geometric Nonlinearities

Nonlinearities in the structure are present due to the downbearing applied by the strings and causing the geometry of the structure to change as it deflects. The stiffness matrix becomes itself a function of the unknown DOF values (Ivančo, 2009) and the Finite Element equation of the discretization process becomes nonlinear such as:

$$[K(u)] \{u\} = \{F_a\} \quad (5.6)$$

where $\{u\}$ represents the vector of unknown DOF and $\{F_a\}$ is the vector of applied loads. An iterative process is therefore needed, such as Newton Raphson method (Kohnke, 1999). Based on NR method, the nonlinear expression in Eqn.5.6 can be re-written as (Kohnke, 1999):

$$[K_i^T] \{\Delta u_i\} = \{F^a\} - \{F_i^{nr}\} \quad (5.7)$$

$$\{u_{i+1}\} = \{u_i\} + \{\Delta u_i\} \quad (5.8)$$

where $[K_i^T]$ is the tangent stiffness matrix at the equilibrium iteration i and $\{F_i^{nr}\}$ is the vector of restoring loads (i.e., corresponding to the element internal loads). $[K_i^T]$ and $\{F_i^{nr}\}$ are both evaluated based on the values given by $\{u_i\}$. The right-hand expression in Eqn.5.7 (i.e., $\{F^a\} - \{F_i^{nr}\}$) is known as the residual (i.e., out-of-balance load vector). The first NR iteration is represented in Figure 5.1. More than one NR iterations are needed to reach the converged solution. The method can be summarized in the following algorithm (Kohnke, 1999):

- **Step 1:** Assume $\{u_0\}$ (i.e., which is the converged solution from the previous time step, on the 1st time step, $\{u_0\} = \{0\}$)
- **Step 2:** Update $[K_i^T]$ and $\{F_i^{nr}\}$ from the configuration $\{u_i\}$
- **Step 3:** Compute $\{\Delta u_i\}$ from Eqn. 5.7
- **Step 4:** Obtain the next iteration $\{\Delta u_{i+1}\}$ by adding $\{\Delta u_i\}$ to $\{u_i\}$
- **Step 5:** Repeat Step 2 to 4 until the convergence is obtained

Figure 5.2 displays the solution of the next iteration $i + 1$ of the example given in

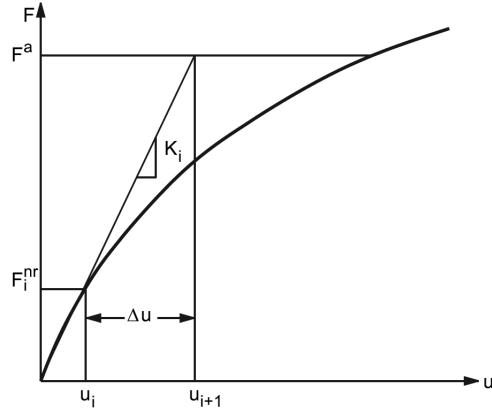


Figure 5.1: First Iteration of NR (Kohnke, 1999)

Figure 5.1. Subsequent iterations proceed following an identical fashion. When the iteration process is over, the obtained solution should correspond to the load level

$\{F^a\}$, and the final converged solution is in a state of equilibrium (i.e., the restoring load vector $\{F_i^{nr}\}$ would equal the applied load vector $\{F_a\}$ within some tolerance). Note that none of the intermediate solutions would reach equilibrium.

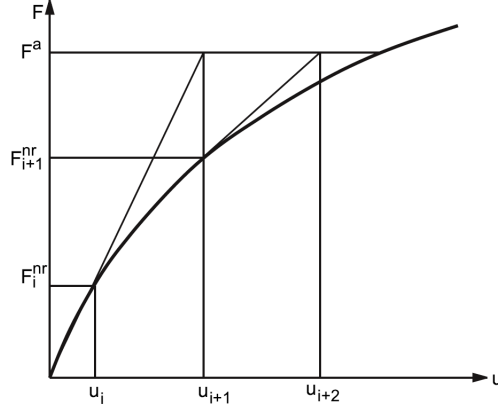


Figure 5.2: Iterations of NR (Kohnke, 1999)

5.3.1 Harmonic Analysis

The harmonic analysis in general is relative to the behavior of a structure subjected to a cyclic loading (Madenci and Guven, 2006). The response due to this type of excitation is hence expected to be cyclic too. For our investigations, harmonic analysis was of most interest when looking at the effects of the structural damping on the material of the soundboard.

In order to accurately represent the board, Sitka Spruce is the wood of choice, as it was detailed in the material properties section (i.e., Chapter 4). This kind of wood is widely chosen by manufacturers for its superior vibrational characteristics. In addition, one of the most important factors in a soundboard's vibrational behavior is its quality factor, noted Q , and which represents how damped is the response of a resonator to an excitation. The quality factor is defined as:

$$Q = \frac{f_0}{\Delta f} = \frac{f_0}{f_2 - f_1} \quad (5.9)$$

where f_0 represents the frequency at which the amplitude of the peak is maximal (Figure 5.3), f_1 and f_2 correspond respectively to the values of the frequencies at the intersections of the FRF curve with the horizontal line at the maximal amplitude of the chosen quantity (e.g., displacement, velocity, acceleration...), divided by $\sqrt{2}$ (i.e., the -3 dB rule) (Blom et al., 1992). Note that $\Delta f = f_2 - f_1$ is called the bandwidth of the frequency peak. As a result, a high quality factor is obtained when the bandwidth is relatively small comparing to the frequency of resonance.

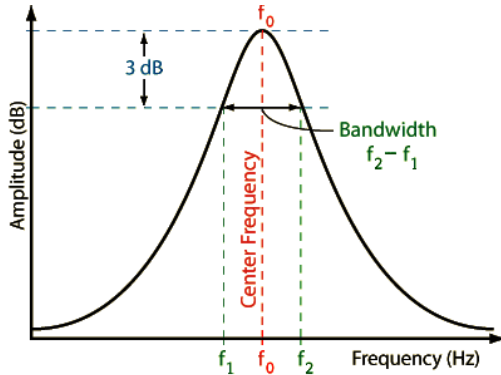


Figure 5.3: FRF Plot Showing the Different Parameters Needed to Compute the Quality Factor Q

When the structural damping of the material is accounted for, another alternative of expressing the quality factor can be given as:

$$Q = \frac{1}{2\zeta} \quad (5.10)$$

It was found that in comparison to other materials, Spruce produces the highest quality factor, which means a lower rate of energy loss in the soundboard (Giordano and Hansen, 2011). In the results section (i.e., Chapter 6), the effects of different values of structural damping on the quality factor will be studied, after generating the Frequency Response Functions by means of harmonic analyses.

5.4 Sensitivity Analysis

The main purpose of sensitivity analysis is to determine which parameters have the largest influence on the soundboard's behavior. For the various sensitivity analyses that will be presented in the results section (i.e., Chapter 6), realistic ranges of the input factors are chosen. An understanding of the significance of these parameters can later be used in the optimization of the soundboard.

5.4.1 Global Sensitivity Techniques

Pearson Linear Correlation Coefficients provide a measure of the linear relationship between two sets of variables (Figure 5.4). For a response y and a set of inputs x , the coefficients can be written as (Ekström, 2005):

$$\rho_{xy} = \frac{\sum_{i=1}^N (y_i - \bar{y})(x_i - \bar{x})}{\sqrt{\sum_{i=1}^N (y_i - \bar{y})^2 \cdot \sum_{i=1}^N (x_i - \bar{x})^2}} \quad (5.11)$$

where \bar{x} and \bar{y} being respectively the means of x and y .

To remedy the disadvantage of Pearson Linear Correlation Coefficients, in case of nonlinear relationships (Figure 5.5), the Spearman Rank Order Correlation is used (Saltelli et al., 2008). This method assesses the type of relationship between two variables providing the monotonicity condition. The data is replaced by its corresponding rank and the correlation coefficients are obtained following the same fashion as in Eqn.(5.11), as follows:

$$\rho_{sr} = \frac{\sum_{i=1}^N (r_i - \bar{r})(s_i - \bar{s})}{\sqrt{\sum_{i=1}^N (r_i - \bar{r})^2 \cdot \sum_{i=1}^N (s_i - \bar{s})^2}} \quad (5.12)$$

These two methods will be tested and the results will be presented and compared in Chapter 6.

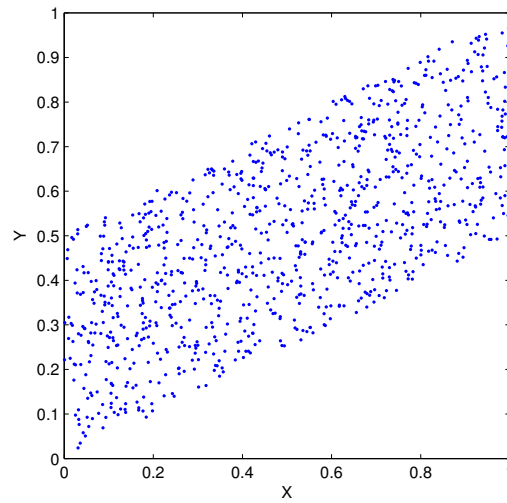


Figure 5.4: Scatter Plot Showing a Linear Relationship Between an Input X and an Output Y

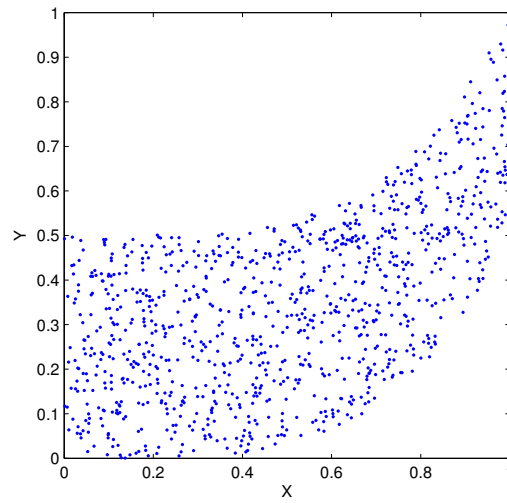


Figure 5.5: Scatter Plot Showing a Nonlinear Monotonic Relationship Between an Input X and an Output Y

5.4.2 Variance Based Techniques

Assuming an output Y and k independent input factors X_i ($1 \leq i \leq k$), the model function can be represented as $Y = f(X)$. Sobol (Sobol, 2001) introduced the variance of the conditional expected value (i.e., $V_i = V[E(Y | X_i)]$) to indicate the effect of a factor X_i on the variance of the output Y .

The “First Order Sensitivity Index” S_i accounts for the main effect contribution. It corresponds to the normalization of V_i by the total variance of the output:

$$S_i = \frac{V[E(Y | X_i)]}{V(Y)} \quad (5.13)$$

A second order effect, providing the coupled effect of the pair X_i, X_j is $V[E(Y | X_i, X_j)]$. Therefore the “Second Order Sensitivity Index” is:

$$S_{ij} = \frac{V[E(Y | X_i, X_j)]}{V(Y)} \quad (5.14)$$

Following an analogical fashion, higher order effects can be determined and the total sensitivity index S_{Ti} relative to an input X_i accounts for the sum of all the indices that are relating to it (Saltelli et al., 2008).

Sobol (Sobol, 2001) proposes to decompose the model function $Y = f(X)$ into summands of increasing dimensionality (Y being the output and $X = X_1 \dots X_k$):

$$f(X) = f_0 + \sum_{i=1}^k f_i(X_i) + \sum_{i=1}^k \sum_{j=i+1}^k f_{ij}(X_i, X_j) + \dots + f_{1\dots k}(X_1 \dots X_k) \quad (5.15)$$

where f_0 is the expected value of the output $f_0 = E(Y)$.

Within Ω_k , the space of inputs, the total variance can be defined as:

$$V(Y) = \int_{\Omega_k} f^2(X) dX - f_0^2 \quad (5.16)$$

Partial variances are computed for $1 \leq i_1 \leq \dots \leq i_s \leq k$:

$$V_{i_1 \dots i_s} = \int f_{i_1 \dots i_s}^2(X_{i_1}, \dots, X_{i_s}) dX_{i_1} \dots dX_{i_s} \quad (5.17)$$

Sensitivity indices can be easily obtained from:

$$S_{i_1 \dots i_s} = \frac{V_{i_1 \dots i_s}}{V(Y)} \quad (5.18)$$

For computation purposes, Matlab Kriging Toolbox DACE (Lophaven et al., 2002) is used to construct a surrogate (i.e., f_{eval}) and approximate the responses $f_0 = E(Y)$ is then estimated using the following Monte Carlo approximation:

$$\hat{f}_0 = \frac{1}{N} \sum_{i=1}^N f_{eval}(X_i) \quad (5.19)$$

The variance $V(Y)$ in Eqn.(5.16) is also approximated by:

$$\hat{V}(Y) = \frac{1}{N} \sum_{i=1}^N f_{eval}^2(X_i) - \hat{f}_0^2 \quad (5.20)$$

The main effect (i.e., $V_i = V[E(Y | X_i)]$) needs also to be approximated. For that, two new sets of Monte Carlo samples are generated as input factors (i.e., X^{s_1} and X^{s_2}), of same size as X (i.e., $N \times k$).

$X_{-i}^{s_1}$ and $X_{-i}^{s_2}$ represent the full sets of X^{s_1} and X^{s_2} , omitting the i_{th} entry respectively (Saltelli, 2002).

Finally, the main effect V_i is written as:

$$\hat{V}_i = \frac{1}{N} \sum_{i=1}^N f_{eval}(X^{s_1}) f_{eval}(X_{-i}^{s_2}, X_i^{s_1}) - \hat{f}_0^2 \quad (5.21)$$

The following procedure is adopted to compute the Sobol indices (Homma and Saltelli, 1996). The input factor set is divided into two separate subsets. The first one includes the variable X_i and the second includes its complementary set (i.e., X_{ci}). The model function can then be decomposed as:

$$f(X) = f_0 + f_i(X_i) + f_{ci}(X_{ci}) + f_{i,ci}(X_i, X_{ci}) \quad (5.22)$$

The total variance of Y becomes:

$$V(Y) = V_i + V_{ci} + V_{i,ci} \quad (5.23)$$

Then, the total effect Sobol index S_{T_i} , which accounts for the sum of all the indices that are relating to X_i (i.e., first order effect and all coupled effects with the rest of the factors) is given by:

$$S_{T_i} = S_i + S_{i,ci} \quad (5.24)$$

Also, by dividing all the terms in Eqn. 5.23 by $V(Y)$, we obtain:

$$1 = \frac{V_i}{V(Y)} + \frac{V_{ci}}{V(Y)} + \frac{V_{i,ci}}{V(Y)} = S_i + S_{ci} + S_{i,ci} \quad (5.25)$$

As a result, using Eqn. 5.24 and Eqn. 5.25, the following relations can be derived:

$$S_{T_i} = S_i + S_{i,ci} \equiv 1 - S_{ci} \quad (5.26)$$

Therefore, to obtain the total Sobol index for a variable X_i , only the complementary index is needed (Ekström, 2005):

$$S_{ci} = \frac{V_{ci}}{V(Y)} \quad (5.27)$$

V_{ci} is obtained following the same analogy as Eqn.(5.21) such that:

$$\hat{V}_{ci} = \frac{1}{N} \sum_{i=1}^N f_{eval}(X^{s_1}) f_{eval}(X_{-i}^{s_1}, X_i^{s_2}) - \hat{f}_0^2 \quad (5.28)$$

Finally, based on the previously detailed method of computation, the Sobol indices were evaluated for various sets of input factors (Chapter 6).

CHAPTER 6

RESULTS

6.1 Introduction

The upcoming sections show the findings obtained after use of the techniques introduced in Chapter 5. The items that will be addressed will deal with the geometric validation of the fully parameterized model (i.e., influence of the soundboard ribs, influence of the variation of the board thickness...), as well as the dynamics (i.e., mainly the effects of crowning, downbearing and boundary conditions on the eigenmodes). The most influential parameters will be found through sensitivity analysis and various configurations will be tested in this context.

To ensure a maximum accuracy among the input factors which can have very different ranges of variation, the variability of any factor X will be scaled into \tilde{X} which varies within an interval [0 - 1], knowing its actual physical range [X_{min} - X_{max}] such as:

$$\tilde{X} = \frac{X - X_{min}}{X_{max} - X_{min}} \quad (6.1)$$

Unless otherwise specified, the features of the piano used in the results section are based on the soundboard of a 2.74 m Steinway Model D grand piano (Steinway, 1934).

6.2 Downbearing: Linear and Geometrically Nonlinear Approaches

Downbearing introduces stresses on the soundboard that are likely to change its modal properties and to make the displacements become quite large. This section

aims at studying the modeling of the piano soundboard with and without geometric nonlinearities.

In order to investigate the influence of geometric nonlinearities, the first and second natural frequencies are studied as functions of the amount of the strings tension (i.e., which is resulting on the downbearing effect). This amount of tension will be varied from a null value (i.e., effects on the strings not accounted for) to the actual computed amount when implementing the strings. The studies are first performed while holding fixed different levels of crown for the board.

A non-crowned soundboard (i.e., initially flat), is considered first (Figure 6.1). The ranges of variation are detailed for the first eigen-mode in Table 6.1. It is then observed from Figure 6.1 and Table 6.1 that, whether the linear or the nonlinear approaches are considered, the eigen-frequencies are only increasing with downbearing for the flat structure. Also, when comparing the two methods, a significant variation is observed. It is clear that the effect of strings tension is mainly noticed for the geometric nonlinear configuration: Over 20% of relative difference between the frequencies of a non-loaded and a maximally loaded board when considering the nonlinear approach.

Table 6.1: Effects of Variation of the Strings Tension on a Flat Soundboard for the 1st Frequency (Hz)

Linear Approach		
Min Freq	Max Freq	Relative variation
53.23	59.28	10.20 %
Nonlinear Approach		
Min Freq	Max Freq	Relative variation
53.24	65.70	23.40 %

The study is next performed on a slightly crowned soundboard having a radius $R_c = 50\text{ m}$ (Figure 6.2 and Table 6.2), an averagely crowned one for $R_c = 35\text{ m}$ (Conklin Jr, 1996a) presented in Figure 6.3 and Table 6.3 and finally a highly crowned

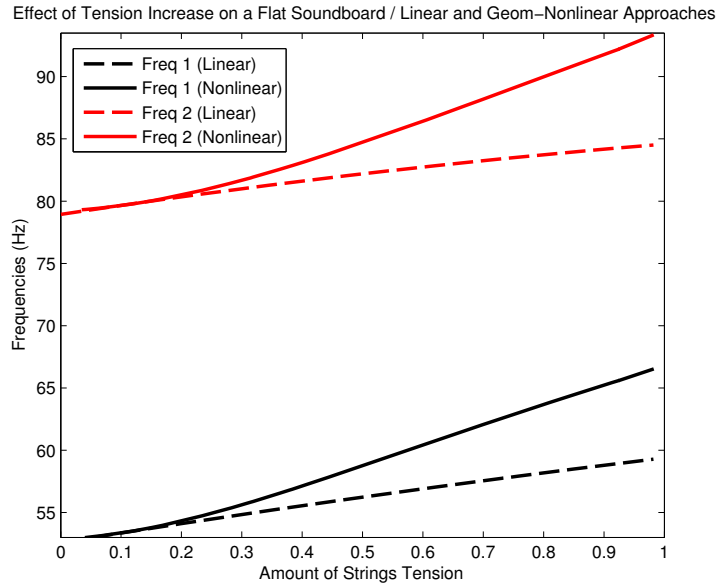


Figure 6.1: Effects of Variation of the Strings Tension on a Flat Soundboard for the 1st and 2nd Frequencies: Linear (Dashed), Geometrically Nonlinear (Solid)

board with a radius $R_c = 15\text{ m}$, for which results are shown in Figure 6.4 and Table 6.4.

When a curvature of radius $R_c = 50\text{ m}$ is introduced, the frequencies are slightly changed for the linear approach. However, with geometric nonlinearities, an increasing trend is clearly depicted.

For an averagely curved board ($R_c = 35\text{ m}$), for the linear case, the natural frequencies are increasing by only 1.71%. For the nonlinear approach, a different situation is numerically observed: The natural frequencies primarily decrease, then start to increase again from approximately half of the actual amount of strings tension, as it can be observed in Figure 6.3. In fact, the first decreasing comes from the global compression introduced by the crowning and which is not compensated by the board when downbearing is not very important (i.e., lower amount of strings tension). Whereas for that same level of crown, when the amount of tension gets

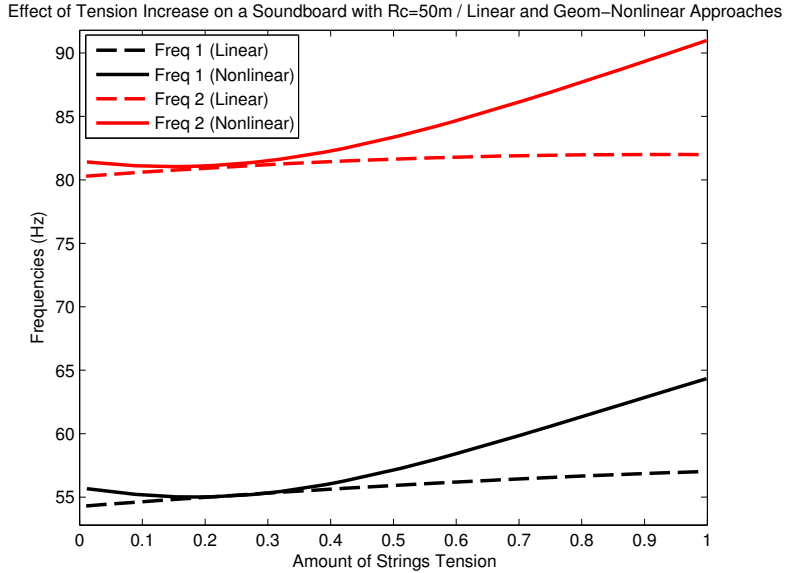


Figure 6.2: Effects of Variation of the Strings Tension with $R_c = 50 \text{ m}$ for the 1st and 2nd Frequencies: Linear (Dashed), Geometrically Nonlinear (Solid)

larger, the increase in frequencies due to the downbearing (i.e., coming from the structure stiffening) can be observed as expected. This means that the minimum downbearing amount is not enough to “overcome” a crown of a radius $R_c = 35 \text{ m}$. It becomes sufficient starting from about half of the actual amount of tension (i.e., when the frequencies start increasing again).

Finally, if the board is highly curved ($R_c = 15 \text{ m}$), the frequencies only decrease for the linear approach as it can be observed in Figure 6.4. For the nonlinear approach, the trend is also decreasing in the beginning. Then, when the tension approaches its actual amount, a slight increase of frequencies is noted. For such a highly crowned board, the actual downbearing amount is required to oppose the crown and to be able to induce the global traction that would normally result in increasing the natural frequencies (Mamou-Mani et al., 2008).

The comparisons made while holding various crown levels proved that the effect

Table 6.2: Effects of Variation of the Strings Tension with $R_c = 50 \text{ m}$ for the 1st Frequency (Hz)

Linear Approach		
Min Freq	Max Freq	Relative variation
54.31	57.01	4.73 %
Nonlinear Approach		
Min Freq	Max Freq	Relative variation
55.66	64.33	15.58 %

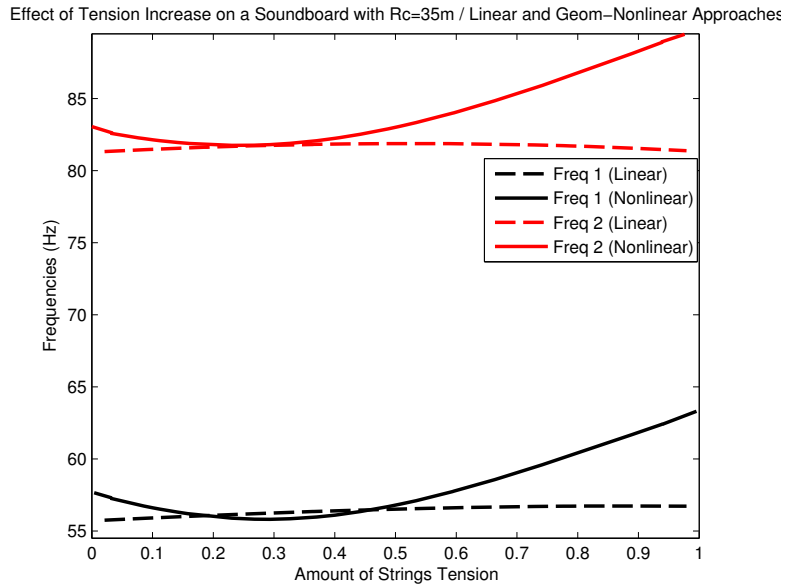


Figure 6.3: Effects of Variation of the Strings Tension with $R_c = 35 \text{ m}$ for the 1st and 2nd Frequencies: Linear (Dashed), Geometrically Nonlinear (Solid)

of downbearing is mainly observed for the geometrically nonlinear configuration. The initial crowning has also an impact on the evolution of the frequencies with downbearing and the difference between the two approaches is more noticeable for higher levels of crowning. Note that the residual stresses introduced during the crowning have not been accounted for.

Table 6.3: Effects of Variation of the Strings Tension with $R_c = 35 \text{ m}$ for the 1st Frequency (Hz)

Linear Approach		
Min Freq	Max Freq	Relative variation
55.75	56.72	1.71 %
Nonlinear Approach		
Min Freq	Max Freq	Relative variation
57.27	62.53	9.18%

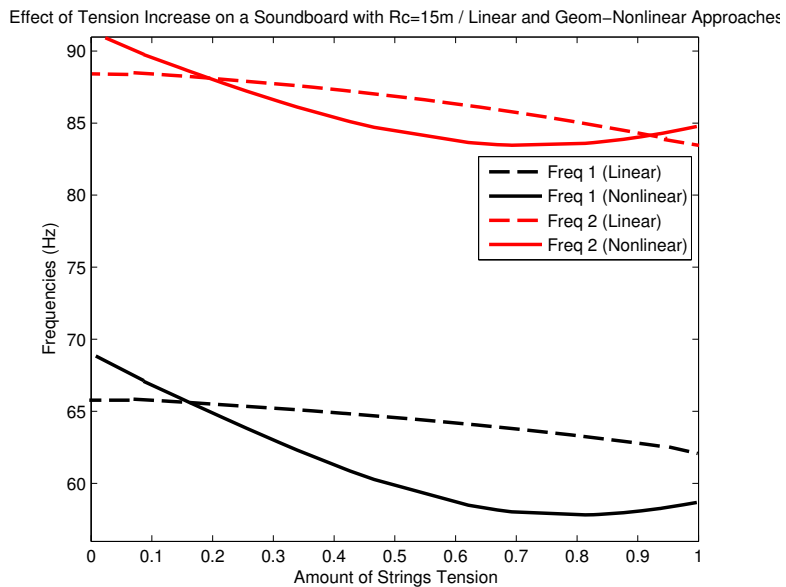


Figure 6.4: Effects of Variation of the Strings Tension with $R_c = 15 \text{ m}$ for the 1st and 2nd Frequencies: Linear (Dashed), Geometrically Nonlinear (Solid)

6.3 Competing Effects of Crowning and Downbearing

The main and coupled effects of crowning and downbearing are studied while including geometric nonlinearities. When downward forces are disregarded (i.e., total strings tension assumed to equal a null value), the effects of varying the curvature

Table 6.4: Effects of Variation of the Strings Tension with $R_c = 15 \text{ m}$ for the 1st Frequency (Hz)

Linear Approach		
Min Freq	Max Freq	Relative variation
65.74	62.61	4.76%
Nonlinear Approach		
Min Freq	Max Freq	Relative variation
69.08	58.51	18.06%

from slightly crowned ($R_c = 50 \text{ m}$) to highly crowned ($R_c = 15 \text{ m}$), on the first two natural frequencies are displayed in Figure 6.5.

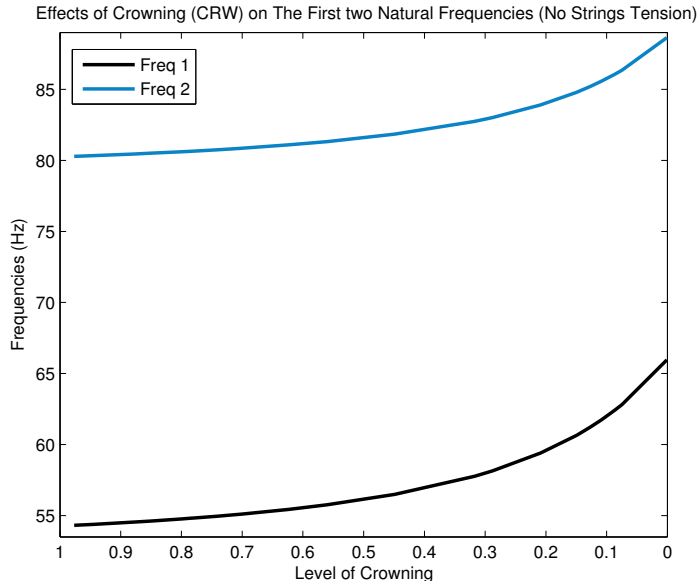


Figure 6.5: Effects of the Crowning Without Accounting for the Strings Tension: First Two Natural Frequencies

It is concluded that the natural frequencies are highly sensitive to the level of crown when downbearing is not accounted for. The increase in natural frequencies becomes more noticeable for a strongly crowned structure, reaching for instance

more than 10 Hz for the first natural frequency.

When downward forces are accounted for (i.e., actual amount of tension is considered), the effects of the crown on the first two natural frequencies from slightly to highly crowned are displayed in Figure 6.6. A different behavior than the non tensioned board is observed. The frequencies decrease when the board gets more crowned. The soundboard is in that case, under compression and the “dome” due to the increase in the level of crown, keeps opposing the downward load.

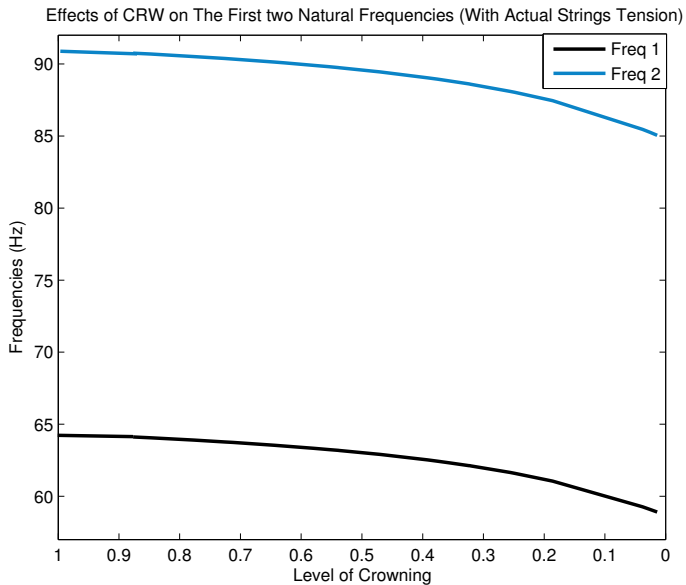


Figure 6.6: Effects of the Crowning when Accounting for the Actual Amount of Strings Tension: First Two Natural Frequencies

To observe the coupled effects of crowning and downbearing and simulate the behavior of an actual soundboard, an averagely crowned board ($R_c = 35\text{ m}$) (Conklin Jr, 1996a) is considered along with downbearing. In addition, structural damping is accounted for, in order to simulate the actual behavior of the wood. The structural damping was documented to have a ratio of $\zeta = 2\%$ (Bucur, 2006). The resulting first three natural frequencies are compared to those relative to a totally

flat structure while including or not the structural damping (Table 6.5 and Table 6.6).

Table 6.5: Coupled Effects of Crowning (CRW) and Downbearing (DWB) for the First Three Natural Frequencies with no Damping (Hz)

Mode	Flat	CRW+DWB (No DMP)	Relative variation
1	53.23	63.21	15.78 %
2	79.97	89.86	11.06 %
3	111.29	119.42	6.80 %

Table 6.6: Coupled Effects of Crowning (CRW) and Downbearing (DWB) for the First Three Natural Frequencies with Damping ($\zeta = 2\%$) (Hz)

Mode	Flat	CRW+DWB (With DMP)	Relative variation
1	53.23	54.47	2.27 %
2	79.97	81.48	1.85 %
3	111.29	112.31	0.90 %

The comparison in Table 6.6 confirms that the soundboard regains an almost “flat curvature” after being subjected to both crowning and downbearing (Chabassier et al., 2010), while including the effects of the structural damping on the material. Consequently, it can be concluded that the loading on the bridges is in opposition with the initial crown and both crowning and downbearing have complementary effects on natural frequencies (Conklin Jr, 1996a). This can be observed graphically using Figure 6.7 which depicts the coupled effects of crowning and downbearing for the first natural frequency.

6.4 Influence of the Nature and Type of the Boundary Conditions

Assuming clamped boundary conditions, the effects of the variation of the lateral width of the boundary area on the three first eigen-frequencies are presented in Table

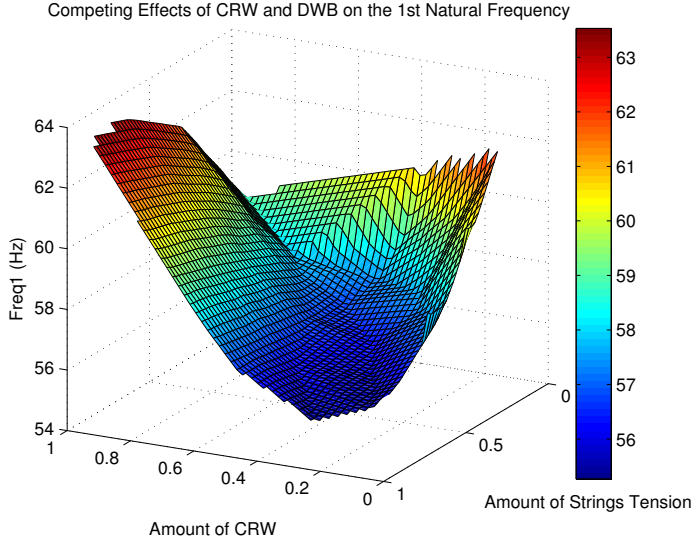


Figure 6.7: Coupled Effects of Crowning and Downbearing on the 1st Natural Frequency

6.7. The width of the boundary area has an important influence on the natural frequencies. The largest the lateral width is, the higher the natural frequencies are. This was expected since a wider boundary implies additional stiffening around the edges and a loss in the flexibility of the structure.

Table 6.7: Frequencies of the First Three Modes for Various Lateral Boundary Widths (Hz)

Mode	$p_b = H_2/100$	$p_b = H_2/50$	$p_b = H_2/25$
1	59.71	63.21	75.20
2	83.59	89.86	103.83
3	110.63	119.42	140.91

To observe the effects of the nature of the boundaries, the lateral width is fixed with $p_b = H_2/50$. Its nature is changed from clamped to simply supported. For this purpose, spring elements have been used (Table 6.8). Obviously, nature of

Table 6.8: Frequencies of the First Three Modes for Various Boundary Conditions (Hz)

Mode	Clamped	Simply Supported	Springs ($K=1e^6 \text{ N/m}$)
1	63.21	60.63	62.94
2	89.86	85.67	88.16
3	119.42	113.55	115.84

the boundaries have a strong impact on natural frequencies since it is directly related to the flexibility of the structure. We note that the configuration using the springs comes in between the clamped and the simply supported. Therefore, it could eventually approximate the actual boundary conditions of the soundboard and it is possible for the user to vary the stiffness K of the springs based on the desired application.

6.5 Effects of the Soundboard Ribs on the Eigen-modes

The ribs (i.e., also called stiffeners or belly bars) are made to strengthen the structure of the soundboard. They are attached to its bottom opposing the bridges and have as function to stiffen the individual planks of the board (Jiang and Giordano, 2004). The ends of the ribs are feathered to avoid the increase in stiffness around the edges and to facilitate the rim fitting (Chabassier and Chaigne, 2011).

Two parameters within the Finite Element model, are relative to the ribs modeling. The first one is the feathering taper ratio r_1 which determines the feathering amplitude and is expressed with respect to the main height of the ribs h_r (see the soundboard scale in Figure 4.2). The second parameter, noted r_2 determines exactly where the section of the ribs should start to be tapered. Figure 6.8 displays two different plots for various feathering starts.

The influence of the variation of the feathering height h_f is studied too. The latest is varied from $h_f = h_r$ (i.e., constant cross section along the ribs) to $h_f = h_r/10$

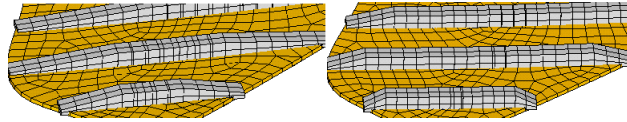


Figure 6.8: Feathered Ribs of the SB with $r_2=1/3$ and $1/8$ (From Left to Right Respectively)

(i.e., highly feathered ribs). Figure 6.9 displays the two configurations.

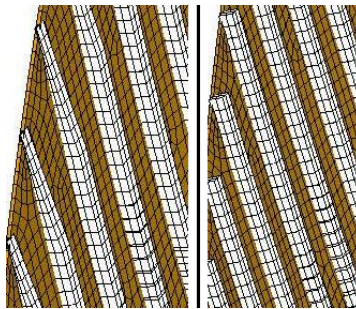


Figure 6.9: Variation of the Feathering Height From $h_f=h_r/10$ (Left) to $h_f = h_r$ (Right)

Table 6.9: Frequencies of the First Five Modes for Different Feathering Heights (Hz)

Mode	$h_f=h_r$	$h_f=h_r/10$	Relative variation
1	85.49	60.25	29.52 %
2	115.78	89.36	22.82 %
3	152.44	120.05	21.24 %
4	159.11	126.12	20.73 %
5	169.56	140.93	16.88%

The variation of h_f produces a very important alteration in the eigen-modes. This can be observed, first, through the values of the first five natural frequencies (Table 6.9) and second, by means of computation of the Modal Assurance Criterion (MAC) that will be introduced briefly: The MAC matrix is a tool used to compare

two vectors to each others. It is widely used in Modal Analysis to compare the eigen-vectors and conclude about the conformity of the mode shapes. The MAC between two mode shape vectors ψ_r and ψ_s is given by (Pastor et al., 2012):

$$MAC(\psi_r, \psi_s) = \frac{(\psi_r^{*T} \cdot \psi_s)^2}{(\psi_r^{*T} \cdot \psi_r) \cdot (\psi_s^{*T} \cdot \psi_s)} \quad (6.2)$$

The MAC approaches the value of unity if ψ_r and ψ_t admit same mode shapes. However, if they are different, its value will be low. MAC matrix was generated for the mode shapes relative to the two different feathering heights stated above (i.e., $h_f = h_r$ and $h_f = h_r/10$). Eigen-modes were confirmed to be highly influenced by the ratio at which the ribs are tapered (Figure 6.10).

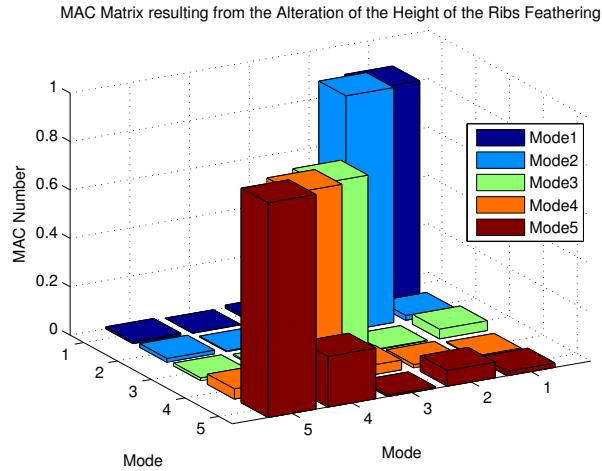


Figure 6.10: MAC Matrix Resulting From the Alteration of the Height of the Ribs Feather

6.6 Influence of the Variation of the Thickness Distribution

The thickness of the board is distributed such that it gets thinner around the edges (Conklin Jr, 1996a). We assume that at the center, the main thickness is defined by t_1 . Around the edges, the parameter is t_2 . Assuming totally clamped boundary

conditions and a lateral width of the boundary area fixed by $p_b = H_2/50$, the influence of the thickness tapering ratio (i.e., $r_3 = \frac{t_2}{t_1}$) is studied for the first three eigen-modes (Table 6.10). Figure 6.11 displays the board while it admits a thickness tapering ratio of $r_3 = \frac{t_2}{t_1} = \frac{1}{3}$.

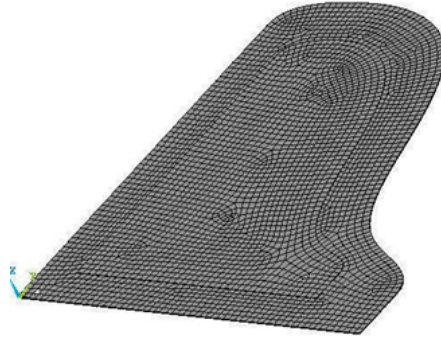


Figure 6.11: Thickness Distribution of the Board For a Taper Ratio $r_3 = 1/3$

Table 6.10: Frequencies of the First Three Modes for Various Tapering Thickness Ratios of the Board (Hz)

Mode	$r_3 = 1/10$	$r_3 = 1/5$	$r_3 = 1/2$
1	55.574	53.645	52.513
2	81.623	79.259	77.892
3	110.710	107.320	105.530

It can be concluded that the variation of the thickness tapering ratio has an important influence on the overall flexibility of the board (Giordano and Hansen, 2011). Note that for the rest of the investigations were r_3 does not need to be varied, the latest will be held fixed to $r_3 = 1/3$, assumed as an average value (Wogram, 1990).

6.7 Sensitivity Analysis Results

6.7.1 Preliminaries

The set of input factors chosen to be studied is a 6D set (Table 6.11), relative to various features of the structure (e.g., geometry, material properties...). Using the specified ranges, Probabilistic Design Analysis of the model was conducted (i.e., using ANSYS Probabilistic Design Module). Monte Carlo sampling was performed to construct the data set.

Table 6.11: 6D Input Factors Set

Input	Range of Variation
Young Modulus of the board E_{Lb}	[9 – 14.17] GPa
Young Modulus of ribs and bridges E_r	[9 – 13.7] GPa
Main thickness of the board t_1	[0.006 – 0.015] m
Height of the ribs h_r	[2 – 4.5] cm
Height of the bridges h_b	[3 – 5.5] cm
Radius of curvature R_c	[15 – 50] m

6.7.2 Pearson Linear Correlation Coefficients (PLCC)

As detailed in Chapter 5, Pearson Linear Correlation Coefficients provide a measure of the linear relationship between two sets of variables. To evaluate the Pearson Linear technique, the first three natural frequencies were observed as outputs. The computed coefficients for the various input factors are presented in Table 6.12.

It is observed that the influencing parameters vary from a frequency to another. The main thickness of the board t_1 is the strongest parameter for the first frequency. However the height of the bridge h_b is more important for the second and third frequencies.

Table 6.12: Pearson Linear Correlation Coefficients for the First Three Natural Frequencies

	1 st Frequency	2 nd Frequency	3 rd Frequency
E_{Lb}	0.0546	0.0571	0.0648
E_r	0.0867	0.1330	0.1807
t_1	-0.2904	-0.4392	-0.2379
h_r	0.1646	0.2961	0.4861
h_b	0.2653	0.4886	0.5131
R_c	0.2484	0.2843	0.2161

6.7.3 Spearman Rank Order Correlation Coefficients (SRCC)

As detailed in Chapter 5, Spearman Rank order Correlation Coefficients provide information about nonlinear relationship between two sets of variables, providing the monotonicity condition. Using Table 6.11 and the first three natural frequencies, bar charts are generated, where the contribution of each input in the variability of the outputs are presented (Figures 6.12, Figures 6.13 and Figures 6.14).

The charts of the Spearman Rank Coefficients confirm the findings of Pearson Correlation Coefficients for the first and second frequencies. However for the third, the height of the ribs h_r is found to be the most impacting instead of the height of the bridges h_b , found by Pearson.

6.7.4 Results of the Variance Based Techniques: Sobol Indices

Following the computational steps that were detailed in Chapter 5, Sobol indices were evaluated for the 6D input parameters in Table 6.11. The first three natural frequencies were chosen as outputs.

First order Sobol indices S_i , complementary Sobol indices S_{ci} , coupled effects Sobol indices $S_{i,ci}$ and the total effects Sobol indices S_{T_i} are represented in Tables 6.13, 6.14 and 6.15, for the 1st, 2nd and 3rd natural frequency respectively.

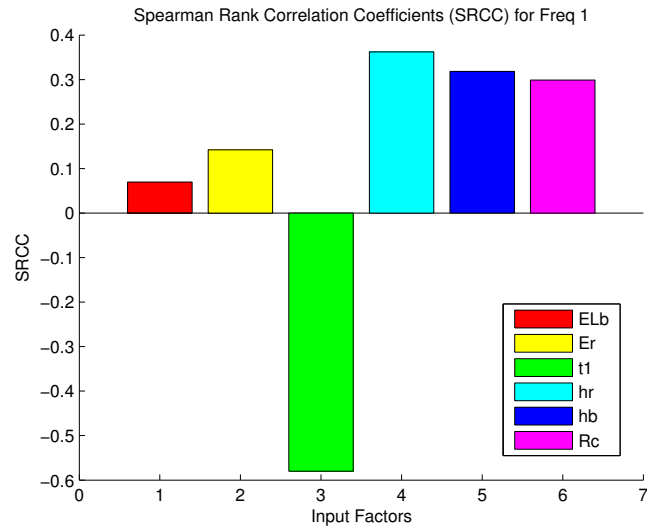


Figure 6.12: Influencing Inputs on the 1st Natural Frequency (by means of Spearman Rank Correlation Coefficients)

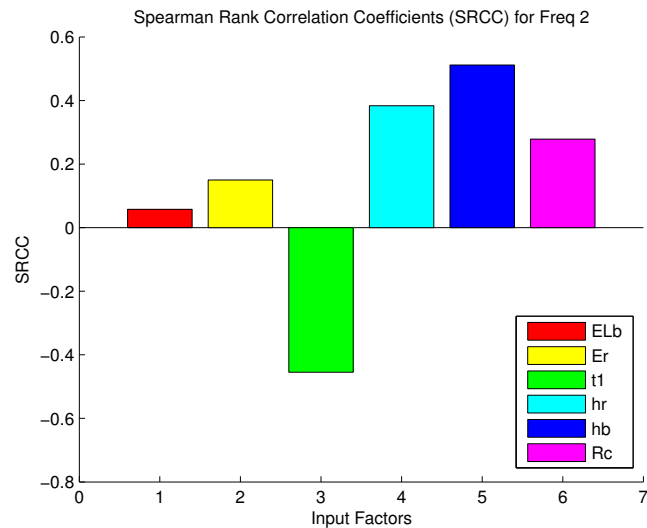


Figure 6.13: Influencing Inputs on the 2nd Natural Frequency (by means of Spearman Rank Correlation Coefficients)

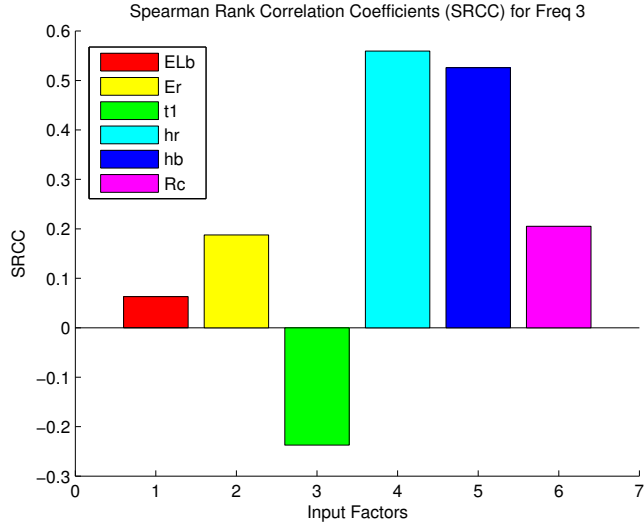


Figure 6.14: Influencing Inputs on the 3rd Natural Frequency (by means of Spearman Rank Correlation Coefficients)

Table 6.13: Sobol Indices for the 1st Natural Frequency

	S_i	S_{ci}	$S_{i,ci}$	S_{T_i}
E_{Lb}	0.0878	0.8035	0.1087	0.1965
E_r	0.0480	0.7114	0.2406	0.2886
t_1	0.2428	0.3861	0.3711	0.6139
h_r	0.2056	0.6649	0.1295	0.3351
h_b	0.0442	0.6489	0.3069	0.3511
R_c	0.0770	0.6006	0.3224	0.3994

Figures 6.15, 6.16 and 6.17 display the contributions of each of the six input factors under the form of percentile portions. These figures show explicitly which parameters have more influence on the variability of the first three natural frequencies.

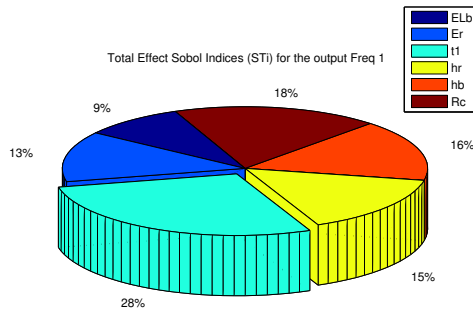
The study of the 6D set with the previously specified ranges, has confirmed that the main thickness of the board t_1 and the height of the bridge h_b are the most

Table 6.14: Sobol Indices for the 2nd Natural Frequency

	S_i	S_{ci}	$S_{i,ci}$	S_{Ti}
E_{Lb}	0.0388	0.8668	0.0944	0.1332
E_r	0.0298	0.8455	0.1247	0.1545
t_1	0.2557	0.4885	0.2558	0.5115
h_r	0.1274	0.7689	0.1036	0.2311
h_b	0.3119	0.5592	0.1289	0.4408
R_c	0.0794	0.7439	0.1767	0.2561

Table 6.15: Sobol Indices for the 3rd Natural Frequency

	S_i	S_{ci}	$S_{i,ci}$	S_{Ti}
E_{Lb}	0.1536	0.8315	0.0150	0.1685
E_r	0.0830	0.8039	0.1131	0.1961
t_1	0.0738	0.5476	0.3786	0.4524
h_r	0.0927	0.4334	0.4740	0.5666
h_b	0.2210	0.6373	0.1417	0.3627
R_c	0.0899	0.8776	0.0324	0.1224

Figure 6.15: Total Effect Sobol Indices for the 1st Natural Frequency

important factors for the first two natural frequencies. These results are explained by the fact that the thickness of the board (i.e., which is tapered around the edges), have a major impact on its overall flexibility. Also, the downbearing is applied on

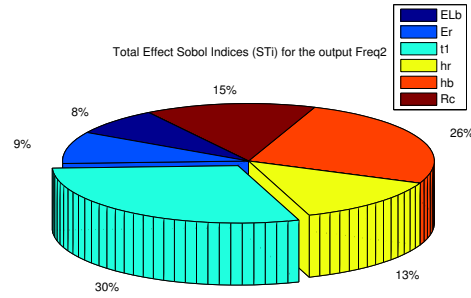


Figure 6.16: Total Effect Sobol Indices for the 2nd Natural Frequency

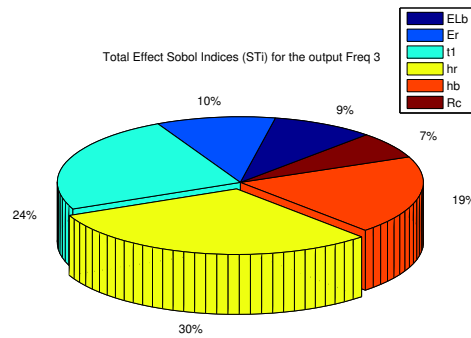


Figure 6.17: Total Effect Sobol Indices for the 3rd Natural Frequency

the bridges at their contact points with the strings, therefore, the height of the bridges was expected to have a large impact on natural frequencies. Finally, for the third eigen-mode, where the height of the ribs h_r was dominating, the board is highly stiffened by the inclusion of the ribs. We note that Sobol indices offer more information about the degree of contribution of an input in the variability of the outputs, since the complementary and coupled effects indices can also be evaluated.

6.8 Harmonic Analyses Results

Harmonic analysis was performed on the soundboard in order to observe the influence of the structural damping on its eigen-modes. Figure 6.18 displays the FRF of the displacements on the z direction with a specified damping ratio of $\xi = 0.02$. It can be observed from Figure 6.18 that the peaks of displacement amplitudes are located at the frequency values depicted by modal analysis (i.e., Table 6.16).

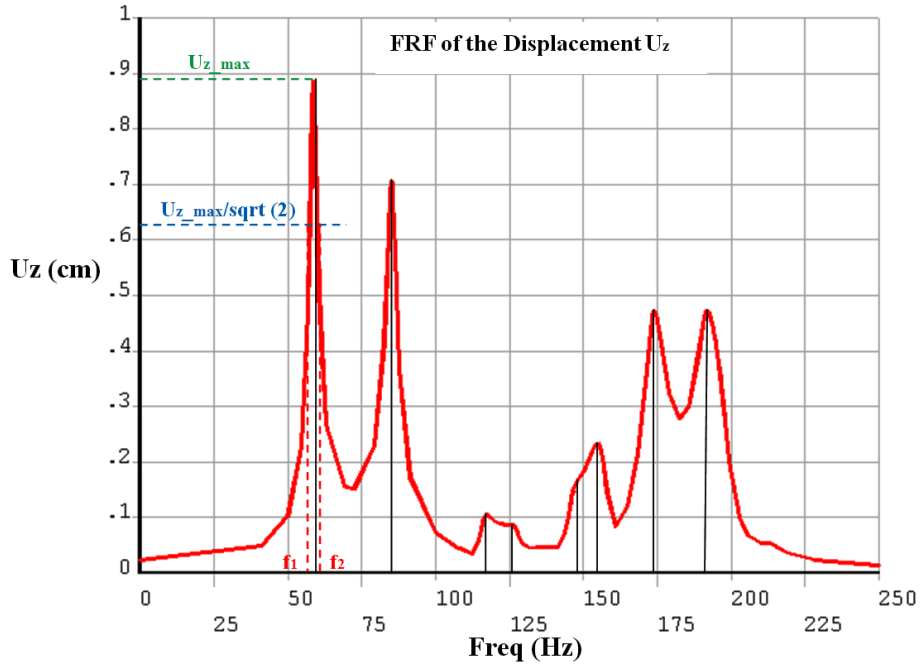


Figure 6.18: FRF of the Displacements on the z Direction (DMP ratio $\xi = 0.02$)

The damping ratio was assigned the value $\xi = 0.02$, which based on Eqn.(5.10) leads to a quality factor $Q = 25$. We propose also to test the -3 dB rule and compute the quality factor based on Eqn.(5.9), using the 1st natural frequency:

$$Q = \frac{f_0}{\Delta f} = \frac{f_0}{f_2 - f_1} = \frac{55.925}{56.931 - 54.670} = 24.73 \quad (6.3)$$

We observe that the computed value is very close to 25 (Eqn.(6.3)).

Table 6.16: Natural Frequencies for DMP Ratio $\xi = 0.02$ (Hz)

Mode	Frequency (Hz)
1	55.925
2	81.287
3	109.610
4	121.180
5	147.300
6	162.470
7	174.890
8	198.670

For a more important damping ratio (e.g., $\xi = 0.04$), the FRF is observed in Figure 6.19. The bandwidths around the frequency peaks are wider and the quality factor Q is computed following the same fashion, to be $Q = 12.5$. We observe that some modes cannot be depicted anymore when the damping ratio is doubled (e.g., the last two modes). The obtained results confirm that a high quality factor is obtained when the bandwidth is relatively small comparing to the frequency of resonance. In addition, when the structural damping ratio gets larger, the quality factor decreases as it was seen for the previous two cases.

6.9 Conclusions

The various modeling techniques introduced in Chapter 5 were performed and different conclusions could be drawn.

The actual consideration of the strings was chosen to account for downbearing. Investigations were about whether or not to represent the downbearing while accounting for geometric nonlinearities. In this context, linear and geometrically nonlinear approaches were tested on different configurations of the soundboard (i.e., variable amounts of downbearing and levels of crown). It was shown that whatever the implemented crown level is, the effects of downbearing on the bridges were

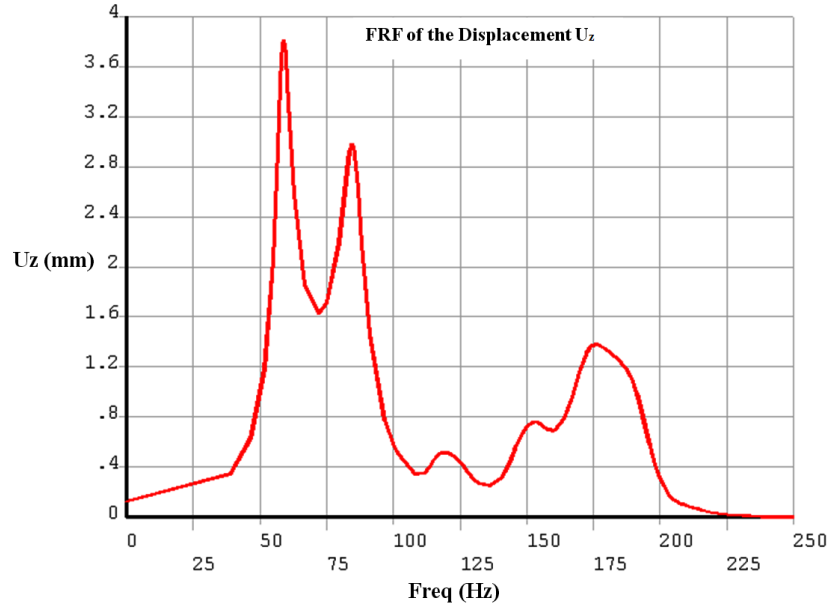


Figure 6.19: FRF of the Displacements on the Z Direction (DMP ratio $\xi = 0.04$)

mainly observed when accounting for geometric nonlinearities (i.e., large displacements assumption), that is why the geometrically nonlinear approach was the one chosen to accurately represent the downward forces. It was also noted that the initial crowning has an important impact on the eigen-modes.

As a matter of fact, observing the competing effects of crowning and downbearing in various configurations, allowed us to conclude that when choosing optimal values for the amount of downward forces and the crown level, the soundboard regains an almost flat curvature, while including the effects of structural damping on the material. That is confirming what was stated in literature.

The types of the boundaries as well as their natures were also of special concern to our research since they have a strong influence on the dynamic behavior of the soundboard. After observing the variations in natural frequencies due to the lateral width of the boundary area or its nature (i.e., from totally clamped to simply supported), spring elements having degrees of freedom along the vertical axis of the

soundboard were implemented to help simulate the actual behavior of the soundboard. This offers the users the choice to model configuration that would match the most their needs.

The soundboard ribs are among the most important components of the structure since they have a strong influence on its stiffening (i.e., which influences highly its modal behavior). Therefore, they were studied closely in order to prove how much varying their characteristics (e.g., the feathering taper ratio and the feathering starting ratio) could affect the mode shapes of the entire soundboard.

The overall thickness of the board plays a major role on its flexibility and its interactions within the surrounding elements (e.g., the rim and the keyboard). The thickness of the board was distributed in a way that it gets thinner around its edges. The influence of that tapering ratio with respect to the main thickness of the board was looked at to show how much this feature could affect the natural frequencies of the soundboard.

A big interest was also brought to the sensitivity analysis since it represents a very powerful tool in distinguishing the most important factors among a set of inputs on the variability of the natural frequencies. Global sensitivity techniques were performed (i.e., Pearson Linear Correlation Coefficients and Spearman Rank Order Correlation coefficients) as well as the variance based techniques (i.e., Sobol indices). Material properties relative to the different components of the soundboard were included and it was shown that those relative to the ribs are the most influencing. For a 6D set of input factors, it was shown that the the thickness of the board t_1 , the height of the bridges h_b and the height of the ribs h_r are the most influencing parameters on the modal outputs (i.e., the first three natural frequencies)

Finally, the results chapter included a harmonic analysis study which was crucial in determining the quality factor of the board and the influence of the consideration of different damping ratios. In this case, the investigations around the modal behavior were based on the Frequency Response Functions.

CHAPTER 7

DISCUSSION AND FUTURE WORK

This thesis presents a fully parameterized Finite Element piano soundboard model. The model allows users to analyze various soundboard shapes and to determine the parameters contributing to the dynamical behavior of the soundboard. These parameters were pointed out by means of sensitivity analysis.

Special concerns were given to downbearing and crowning, in order to understand their mechanical interactions. The effects of crowning and downbearing were studied separately then combined. Based on the study of the natural frequencies of the soundboard, it was confirmed that, for downbearing to be modeled accurately, the inclusion of geometric nonlinearities is needed. To account for downbearing effects, the strings were implemented in the model and their impacts on the bridges were accounted for. The influence of downbearing was measured in the sensitivity analysis by modifying the height of the bridges.

When looking at the soundboard, the crown is most likely non-detectable. However, It was shown that it has a major role in the vibrational behavior of the soundboard, since it helps the structure resist to the downbearing forces applied from the strings. Crowning and downbearing have competing effects, and in some configurations, lead to approximately the same behavior as a flat soundboard without downbearing.

The modeling parameters of the soundboard were studied by means of sensitivity analysis. Pearson Linear and Spearman Rank Correlation Coefficients were computed. Also, variance based techniques were tested using Sobol indices. Thickness of the board and the heights of ribs and bridges proved to have big effects on the eigen-modes comparing to the rest of the parameters.

The importance of accounting for the structural damping of the wood was made clear through a harmonic analysis and by observing the Frequency Response Functions and computing the quality factors.

As expected, the nature of the boundary conditions and the lateral width of the boundary area have a strong influence on the natural frequencies of the soundboard. Various modeling and analysis techniques were performed in order to test the efficiency of the constructed model and its ability to adjust any user defined parameters, with a flexibility in specifying the nature of the boundaries.

Some additional considerations may make the model a more accurate optimization tool. From an acoustical point of view, as an improvement, a solid understanding of vibroacoustics may be an important step in the amelioration of the proposed work. Future study will also consider the inclusion of residual stresses due to crowning. Higher modes will also be investigated and larger input sets for sensitivity analysis will be studied.

APPENDIX A

CHOICE OF THE MESH SIZE

After choosing the real constants for each element, the soundboard components need to be meshed appropriately. The mesh density (i.e., the size or the division within the element edge length) is a very important factor of the model that needs to be considered. If the mesh density is too coarse, the results will include multiple errors. Whereas, if it is too fine, the model would be of a very high cost and large to be run in a standard computer. The evolution of the natural frequencies were then monitored to determine the balance between a coarse and fine mesh before the final one is run. Table A.1 displays the evolution of the first five natural frequencies while refining the mesh size.

Table A.1: Convergence of the First Five Natural Frequencies with Respect to the Mesh Size (Hz)

Mesh Size (Length Division)	Freq 1	Freq 2	Freq 3	Freq 4	Freq 5
0.1	58.64	87.36	120.87	124.41	151.50
0.08	59.64	84.17	118.72	126.99	149.48
0.06	56.88	82.05	111.23	120.11	138.40
0.05	55.88	80.74	115.20	118.39	136.92
0.04	57.62	83.91	113.94	121.23	140.14
0.03	57.03	83.37	113.85	121.52	139.52
0.02	57.96	82.29	112.29	121.44	139.21

From Figure A.1, it can be observed that the natural frequencies keep fluctuating for a coarser mesh, then starting from a size a little bigger than 0.04, the frequencies start to stabilize and to converge to a unique value. Therefore, the generated results within our model were performed for a mesh size of 0.04. The zoom presented in

Figure A.2 shows that the frequencies are already converging for this value and that it is accurate to choose it.

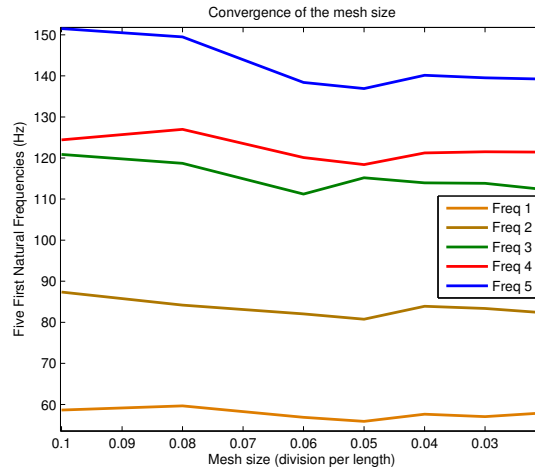


Figure A.1: Convergence of the First Five Natural Frequencies with Respect to the Mesh Size

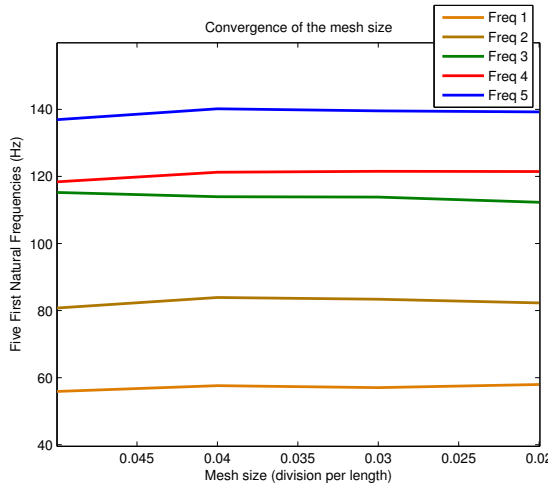


Figure A.2: Convergence of the First Five Natural Frequencies with Respect to the Mesh Size: Zoom on the Convergence Zone

APPENDIX B

DOWNBEARING: COMPARISON BETWEEN THE TWO IMPLEMENTATION TECHNIQUES

We recall that, as detailed in Chapter 4:

- Method 1: First iteration technique.
- Method 2: Actual representation of the strings.

Natural frequencies were compared for the two methods in the cases of a slightly crowned (i.e., $R_c = 50\ m$), an averagely crowned (i.e., $R_c = 35\ m$) and a highly crowned (i.e., $R_c = 15\ m$) board. Results are presented in Table B.1, Table B.2 and Table B.3 respectively.

Table B.1: Comparison Between the Downbearing Implementation Techniques for $R_c = 50\ m$ For the First Five Natural Frequencies (Hz)

Mode	Method 1	Method 2	Relative Variation
1	54.742	54.875	0.243 %
2	80.408	80.606	0.246 %
3	109.110	109.200	0.082 %
4	121.800	120.870	0.763 %
5	137.820	136.890	0.747 %

It can be observed that the relative difference remains lower than 1 % for a slightly crowned soundboard, however it starts increasing for some modes for $R_c = 35\ m$ (e.g., modes 3 and 5), until it reaches almost 4 % for a highly crowned board. This variation in natural frequencies between the two techniques was expected since for the first method, the assumption is based on one iteration which provides a first-order approximation of the deflection due to the strings. This approximation

Table B.2: Comparison Between the Downbearing Implementation Techniques for $R_c = 35\text{ m}$ For the First Five Natural Frequencies (Hz)

Mode	Method 1	Method 2	Relative Variation
1	54.539	54.170	0.681 %
2	80.365	81.220	0.153%
3	109.000	111.850	2.548 %
4	121.410	122.160	0.614 %
5	137.240	140.290	2.174 %

Table B.3: Comparison Between the Downbearing Implementation Techniques for $R_c = 15\text{ m}$ For the First Five Natural Frequencies (Hz)

Mode	Method 1	Method 2	Relative Variation
1	60.183	62.519	3.736 %
2	84.467	86.981	2.890%
3	111.870	115.890	3.469%
4	122.360	125.740	2.688%
5	137.000	141.190	2.967 %

is therefore very rough with potentially large errors. Hence, the implementation of the strings, has proven to be satisfactory and the one iteration technique was just used for comparison purposes.

APPENDIX C

MODAL SHAPES AND NODAL SOLUTIONS FOR THE FIRST SEVEN
EIGEN-MODES

The purpose of the following Appendix is to visualize the deformed shapes as well as the displacement nodal solutions relative to the first seven eigen-modes of the soundboard.

Figure C.1 displays the deformed shapes.

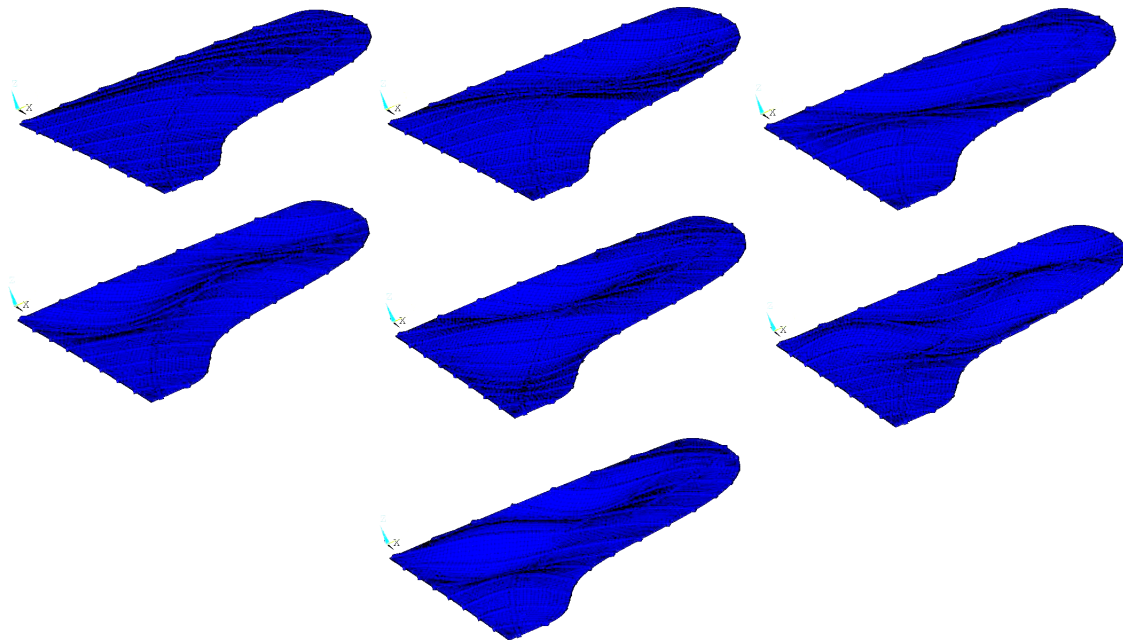


Figure C.1: Deformed Shapes Relative to the First Seven Eigen-modes: From Mode 1 (Top Left) to Mode 7 (Bottom) Respectively.

Also it is possible to observe the nodal displacements in Figure C.2.

Within the results section, only the three first mode shapes were studied, therefore more modes are expanded in this Appendix.

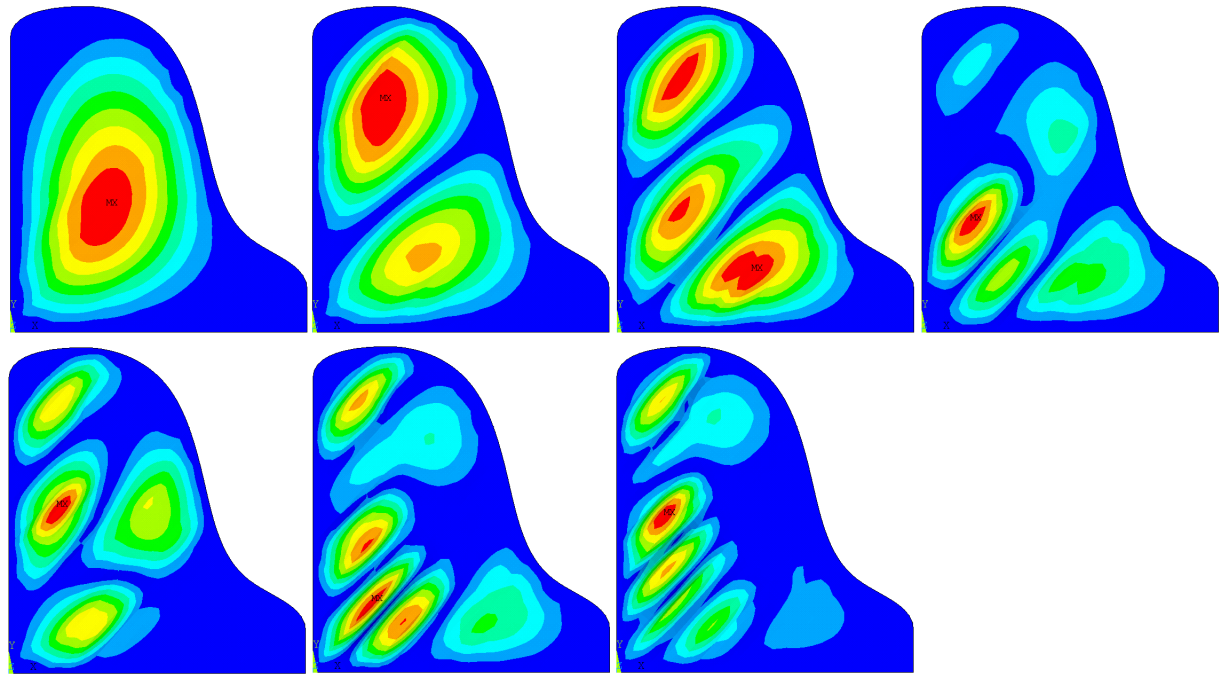


Figure C.2: Nodal Displacements Relative to the First Seven Eigen-modes

APPENDIX D

MODE SHAPES VS. CHLADNI PATTERNS

The mode shapes corresponding to the configuration specified in Table 6.6 are compared to the Chladni patterns obtained by Conklin (Conklin Jr, 1996a), after conducting an experiment on a 2.74 m grand piano soundboard. Figure D.1 shows that the Chladni patterns and the mode shapes from the Finite Element model admit a high level of conformity in the overall features of the presented modes (i.e., the first three mode shapes).

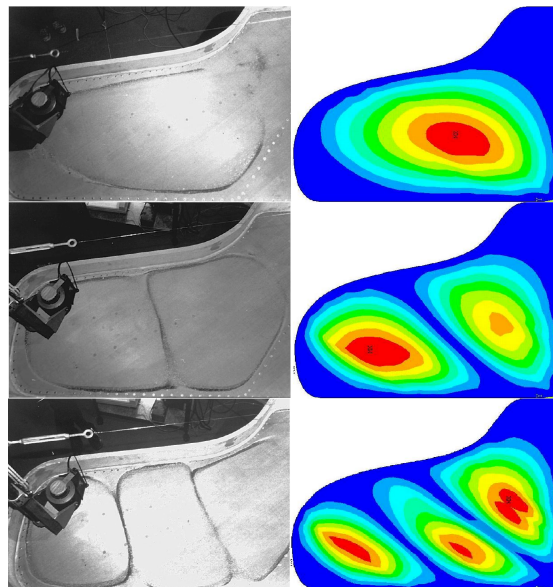


Figure D.1: Chladni Patterns (Conklin Jr, 1996a) Vs. FEM Mode Shapes For the First Three Natural Frequencies

REFERENCES

- Berthaut, J., M. Ichchou, and L. Jezequel (2003). Piano soundboard: structural behavior, numerical and experimental study in the modal range. *Applied Acoustics*, **64**(11), pp. 1113–1136.
- Bilhuber, P. H. and C. Johnson (1940). The influence of the soundboard on piano tone quality. *The Journal of the Acoustical Society of America*, **11**(3), pp. 311–320.
- Blackham, E. (1965). The physics of the piano. *Scientific american*, **213**, pp. 88–99.
- Blom, F., S. Bouwstra, M. Elwenspoek, and J. Fluitman (1992). Dependence of the quality factor of micromachined silicon beam resonators on pressure and geometry. *Journal of Vacuum Science & Technology B: Microelectronics and Nanometer Structures*, **10**(1), pp. 19–26.
- Bucur, V. (2006). Acoustics of wood. *The Journal of the Acoustical Society of America*, **119**(6), pp. 3506–3506.
- Chabassier, J. (2012). *Modélisation et simulation numérique d'un piano par modèles physiques*. Ph.D. thesis, Ecole Polytechnique X.
- Chabassier, J. and A. Chaigne (2011). Modeling and numerical simulation of a piano. *The Journal of the Acoustical Society of America*, **129**, p. 2542.
- Chabassier, J., A. Chaigne, et al. (2010). Modeling and numerical simulation of a nonlinear system of piano strings coupled to a soundboard. In *Proceedings of 20th International Congress on Acoustics, ICA 2010*.
- Clark, J. F. (1998). *A study of the curricula of the high school electronic piano laboratories in the area of Chicago, Illinois to determine any patterns of curriculum design*. Ph.D. thesis, Governors State University.
- Conklin, H. et al. (1996). Design and tone in the mechanoacoustic piano. Part I. Piano hammers and tonal effects. *The Journal of the Acoustical Society of America*, **99**, p. 3286.
- Conklin Jr, H. (1996a). Design and tone in the mechanoacoustic piano. Part II. Piano structure. *The Journal of the Acoustical Society of America*, **100**, p. 695.

- Conklin Jr, H. (1996b). Design and tone in the mechanoacoustic piano. Part III. Piano strings and scale design. *The Journal of the Acoustical Society of America*, **100**, p. 1286.
- Ege, K. (2009). *La table d'harmonie du piano—Études modales en basses et moyennes fréquences (The piano soundboard—Modal studies in the low-and midfrequency ranges), ch. 1 (in English), sec. 2*. Ph.D. thesis, École polytechnique, Palaiseau, France.
- Ege, K., X. Boutillon, and M. Rébillat (2012). Vibroacoustics of the piano soundboard:(Non) linearity and modal properties in the low-and mid-frequency ranges. *Journal of Sound and Vibration*.
- Ekström, P. (2005). A Simulation Toolbox for Sensitivity Analysis. *Masters Degree Project, Faculty of Science and Technology, Uppsala Universitet*.
- Fletcher, N. H. and T. D. Rossing (1998). *The physics of musical instruments*. Springer Verlag.
- Giordano, N. (1997). Simple model of a piano soundboard. *The Journal of the Acoustical Society of America*, **102**, p. 1159.
- Giordano, N. J. and U. J. Hansen (2011). Physics of the Piano. *Physics Today*, **64**(4), p. 58.
- Homma, T. and A. Saltelli (1996). Importance measures in global sensitivity analysis of nonlinear models. *Reliability Engineering & System Safety*, **52**(1), pp. 1–17.
- Ivančo, D. (2009). Introduction to Nonlinear finite element analysis.
- Jiang, M. and N. Giordano (2004). Physical Modeling of the Piano. *EURASIP Journal on Advances in Signal Processing*, **2004**.
- Keane, M. (2006). *An evaluation of piano sound and vibration leading to improvements through modification of the material properties of the structure*. Ph.D. thesis, ResearchSpace@ Auckland.
- Kindel, J., I. Wang, et al. (1987). Vibrations of a piano soundboard: Modal analysis and finite element analysis. *The Journal of the Acoustical Society of America*, **81**(S1), pp. S61–S61.
- Kohnke, P. (1999). *ANSYS theory reference*. Ansys.

- Kopač, J. and S. Šali (2003). Wood: an important material in manufacturing technology. *Journal of materials processing technology*, **133**(1), pp. 134–142.
- Lophaven, S., H. Nielsen, and J. Søndergaard (2002). *DACE: A Matlab kriging toolbox*. Citeseer.
- Madenci, E. and I. Guven (2006). *The Finite Element Method and Applications in Engineering Using Ansys*. Springer.
- Mamou-Mani, A. (2007). *Précontraintes et vibration des tables d'harmonie: vers une modélisation du savoir-faire des fabricants d'instruments de musique*. Ph.D. thesis.
- Mamou-Mani, A., J. Frelat, and C. Besnainou (2008). Numerical simulation of a piano soundboard under downbearing. *The Journal of the Acoustical Society of America*, **123**, p. 2401.
- Mamou-Mani, A., J. Frelat, and C. Besnainou (2009). Prestressed soundboards: analytical approach using simple systems including geometric nonlinearity. *Acta Acustica united with Acustica*, **95**(5), pp. 915–928.
- Moore, T. R. and S. A. Zietlow (2006). Interferometric studies of a piano soundboard. *The Journal of the Acoustical Society of America*, **119**, p. 1783.
- Ortiz-Berenguer, L., F. Casajus-Quiros, and D. Ibanez-Cuenca (2008). Modeling of piano sounds using FEM simulation of soundboard vibration. *Journal of the Acoustical Society of America*, **123**(5), p. 3806.
- Overs, R. E. (2012). Improvements in Piano Construction. EP Patent 2,476,111.
- Pastor, M., M. Binda, and T. Harčarik (2012). Modal Assurance Criterion. *Procedia Engineering*, **48**, pp. 543–548.
- Rumsey, D. and C. Hanggi (2008). The Origins of Seewen's Welte-Philharmonie. *DIAPASON-CHICAGO-*, **1180**, p. 24.
- Saltelli, A. (2002). Making best use of model evaluations to compute sensitivity indices. *Computer Physics Communications*, **145**(2), pp. 280–297.
- Saltelli, A., M. Ratto, T. Andres, F. Campolongo, J. Cariboni, D. Gatelli, M. Saisana, and S. Tarantola (2008). *Global sensitivity analysis: the primer*. Wiley-Interscience.

- Schott, H. (1993). Early Keyboard Instruments. *Revue de Musicologie*, **79**(2), pp. 368–375.
- Schuck, O. and R. Young (1973). Observations on the vibrations of piano strings. *The Journal of the Acoustical Society of America*, **15**, p. 1.
- Sobol, I. (2001). Global sensitivity indices for nonlinear mathematical models and their Monte Carlo estimates. *Mathematics and computers in simulation*, **55**(1-3), pp. 271–280.
- Steinway, T. (1934). Piano construction. US Patent 1,965,360.
- Stulov, A. (2005). Piano string scale optimization on the basis of dynamic modeling of process of the sound formation. *Sound and Vibration*, **11**, p. 14.
- Suzuki, H. (1986). Vibration and sound radiation of a piano soundboard. *The Journal of the Acoustical Society of America*, **80**, p. 1573.
- Tippner, J. (2007). Thermal and moisture straining of grand piano soundboard.
- Tippner, J., P. Koňas, and V. Dániel (2006). Influence of factors on dynamical behaviour of piano soundboard. *Wood Structure and Properties' 06*, p. 417.
- Wogram, K. (1990). *The strings and the soundboard*.
- Young, R. W. (1992). Inharmonicity of plain wire piano strings. *The Journal of the Acoustical Society of America*, **24**, p. 267.